

**THE UNIVERSITY OF WESTERN ONTARIO
DEPARTMENT OF CIVIL AND
ENVIRONMENTAL ENGINEERING**

Water Resources Research Report

**A comprehensive framework
for regional floodplain mapping**

**By:
Mohit P. Mohanty
and
Slobodan P. Simonovic**

**Report No: 109
Date: June 2020**

ISBN: (print) 978-0-7714-3147-0; (online) 978-0-7714-3148-7



A comprehensive framework for regional floodplain mapping



by

Mohit P. Mohanty

and

Slobodan P. Simonovic

**Department of Civil and Environmental Engineering,
Western University, Canada**

Report No. 109

June 2020

Executive summary

In the recent years, there has been a significant global rise in economic damages and human loss from floods. To add to the debatable topic, many reports and studies warn that the situation will become more severe due to consequences from climate change and socio-economic changes. In order to address this global issue, floodplain mapping is considered as a viable option, which can help us identify possible locations at different degrees of risk. However, modelling such extreme events never used to be a simple task for large regions, until recently with the release of global datasets and comprehensive global flood models. The global datasets are increasingly produced by various organisations and made available to the general public. On the other hand, several studies have tried to form global flood models, which consider global hydrological and topographic data to derive high resolution floodplain maps. With these opportunities in hand, it has now become easier than before to perform floodplain mapping at large scales.

The present report describes the past challenges and ongoing efforts on large scale floodplain mapping. A generic framework to produce high-resolution floodplain maps by utilising freely available global products is introduced. Various sources which contain freely available meteorological, hydrological, and topographic data, are also mentioned. The widely used and robust CaMa-Flood hydrodynamic model, its structure and mode of functioning is described in detail. To demonstrate the idea of flood-plain mapping, the NARR reanalysis data for Canada is considered as an input to CaMa-Flood model. The implementation has been performed on Shared Hierarchical Academic Research Computing Network (SHARCNET) platform to be able to complete simulations within a manageable time-frame. The report provides crucial information on data sources, and flood inundation modelling techniques to any water professional working in the area of floodplain mapping.

Keywords: Global flood model; Floodplain mapping; Flood risk; reanalysis.

Table of Contents

Executive summary.....	ii
Table of Contents.....	iii
List of Figures.....	v
List of Tables.....	vi
Chapter 1.....	7
Introduction.....	7
1.1 Impacts of floods – ‘Global context’.....	7
1.2 Impacts of floods- ‘The Canadian story’.....	9
1.2.1 Status of floodplain mapping in Canada: Recent developments.....	10
1.3 Challenges in floodplain mapping over large regions.....	11
1.3.1 Big data handling and large scale flood inundation mapping.....	12
1.3.2 Publicly available datasets.....	15
1.4 Past efforts on floodplain mapping by utilising reanalysis datasets.....	15
1.5 Past efforts on floodplain mapping by utilising global topographic datasets.....	16
Chapter 2 Proposed Floodplain Mapping Framework.....	19
2.1 Run-off observations.....	20
2.2 Catchment-based Macro-scale Floodplain (CaMA-Flood) Model.....	20
2.2.1 Components of the model.....	21
2.2.2 Model structure.....	22
2.3 Validation of floodplain maps.....	26
Chapter 3 Floodplain Mapping Methodology.....	28
3.1 Extraction of runoff data from reanalysis datasets.....	28
3.2 Preparation of input files for CaMa-Flood model.....	28
3.3 Model simulation.....	29
3.4 Outputs processing.....	32
3.5 Conversion of outputs to GeoTIFF format.....	32
3.6 Validation of floodplain maps.....	32
Chapter 4 Sample model simulation and analysis.....	34
4.1 Downloading NARR reanalysis.....	34
4.2 Accessing reanalysis data.....	35
4.3 Extracting runoff values for AoI.....	36
4.4 Converting input runoff from numeric to binary format.....	37
4.5 Model simulations.....	37

Chapter 5 Closing remarks.....	42
Chapter 6 References	43
Appendix A: List of freely available global data in floodplain mapping	51
Appendix B: List of widely used reanalysis datasets.....	54
Appendix C: Previous Reports in the Series.....	56

List of Figures

Figure 1.1: Map of relative changes in population exposed to 1 in 100 floods over changes in total population, 1970–2010 (Source: Jongman et al. (2012), <i>Global Environmental Change</i>).	8
Figure 1.2: The relationship between the global temperature increase from the pre-industrial level (1850-1900) and potential flood consequences under the RCP8.5 scenario (Source: Kinoshita et al. (2018), <i>Environmental Research Letters</i>).	8
Figure 1.3: Trend in number of flooding events in Canada (Source: Public safety Canada, 2017)	9
Figure 1.4: Floodplain Mapping Framework (Source: Federal Floodplain mapping Framework, Version 2.0 2018, Natural Resources Canada)	11
Figure 1.5: A representative illustration of floodplain map (Source: Haznet, 2019)	12
Figure 2.1: A generic framework of flood plain mapping and quantification of population exposure using freely available datasets and global CaMa-Flood model.	19
Figure 2.2: (a) Illustration of a river channel reservoir and a floodplain reservoir defined in each grid	23
Figure 3.1: WinSCP window login window	29
Figure 3.2: PuTTY configuration window	30
Figure 3.3: Connecting to SHARCNET	30
Figure 3.4: Commands to set the modules and paths in Mkinclude file	31
Figure 3.5: Code to submit the jobs in PuTTY and run the code on SHARCNET	31
Figure 3.6: ArcGIS 10.6 administrator	33
Figure 4.1: NARR runoff data: (a) data availability at ftp://ftp.cdc.noaa.gov/Datasets/NARR/monolevel/ ; (b) Index of datasets; and (c) runoff files from 1979 to 2020.	34
Figure 4.2: R code for accessing and extracting NARR NetCDF reanalysis files.	35
Figure 4.3: R code for interpolation.	36
Figure 4.4: R code for interpolation (contd.)	36
Figure 4.5: R code for extracting runoff grids lying within Canada.	36
Figure 4.6: R code for converting input runoff from numeric to binary format.	37
Figure 4.7: Transferring input files to the CaMa-Flood package in input folder.	38
Figure 4.8: Logging into SHARCNET for accessing Graham server.	38
Figure 4.9: Code compilation and creating executables in SHARCNET.	38
Figure 4.10: Final code for running CaMa-Flood model simulation in PuTTY software.	39
Figure 4.11: Flood simulation outputs.	39
Figure 4.12: R code for converting binary data to GeoTIFF format.	40
Figure 4.13: Floodplain map of 2010 for Canada by using NARR reanalysis runoff.	41

List of Tables

Table 1.1: A list of widely used global flood models.....	14
Table 1.2: A list of freely available global data in floodplain mapping.....	17
Table 2.1: Parameters and variables in CaMa-Flood model.	24
Table 3.1: List of directories in the CaMa-Flood package (version 3.6.2).	29
Table 3.2: List of floodwater related outputs generated from CaMa-flood simulation	32
Table A1. List of freely available global data in floodplain mapping.....	50

Chapter 1

Introduction

Several regions of the World experience an elevated risk from riverine flooding, aggravated with concomitant climate change and alterations in socio-economic dynamics (Shao et al., 2016; Ntajal et al., 2017). Under such conditions, there lies a major challenge to comprehensively perform floodplain mapping, which can facilitate building flood mitigation infrastructures, improve land use/urban planning, and prioritizing emergency response strategies. Floodplain mapping is a complex process, not just because it is data-intensive but also involves several sensitive parameters in its formulation. The process becomes more challenging for large regions due to the involvement of computational complexity and requirement of extensive data inputs.

1.1 Impacts of floods – ‘Global context’

Global flood events have increased significantly in the past few decades, resulting in severe human and economic damages (Jongman et al., 2012; Winsemius et al., 2016). Over the period 1980-2018, there were 5,997 disastrous events worldwide, which caused an economic loss beyond a whopping \$1 trillion and approximately 223,482 fatalities (Munich Re, 2018). A recent report by UNISDR (2015) highlights that a population of around 800 million worldwide resides in flood-prone areas, and on an average, about 70 million of them are exposed to floods annually. In a detailed analysis, Jongman et al. (2012) reported that over the period 1970-2010 the number of people exposed to flooding globally has increased by 2.7% more than total population growth (**Figure 1.1**). This value is 4.7% for coastal flooding and 2.6% for riverine flooding. The situation is particularly serious for developing countries, which experienced the largest increase in exposure relative to total population, and on top of that have limited flood protection capacities.

A number of scientific findings further warn that the situation would be aggravated in the near-future with anticipated socio-economic changes (Feyen et al., 2012; Rojas et al., 2013; Mokrech et al., 2015) and associated climate change impacts (Milly et al., 2002; Bouwer et al., 2010; Arnell and Hughes, 2014; Aleiri et al., 2018). In a recent study, Kinoshita et al. (2018) reported on the relationship between the global temperature increase from the pre-industrial

level (1850-1900) and potential flood consequences under the RCP 8.5 scenario and three Socioeconomic Shared Pathways (SSPs; SSP1, SSP2 and SSP3) as illustrated in **Figure 1.2**.

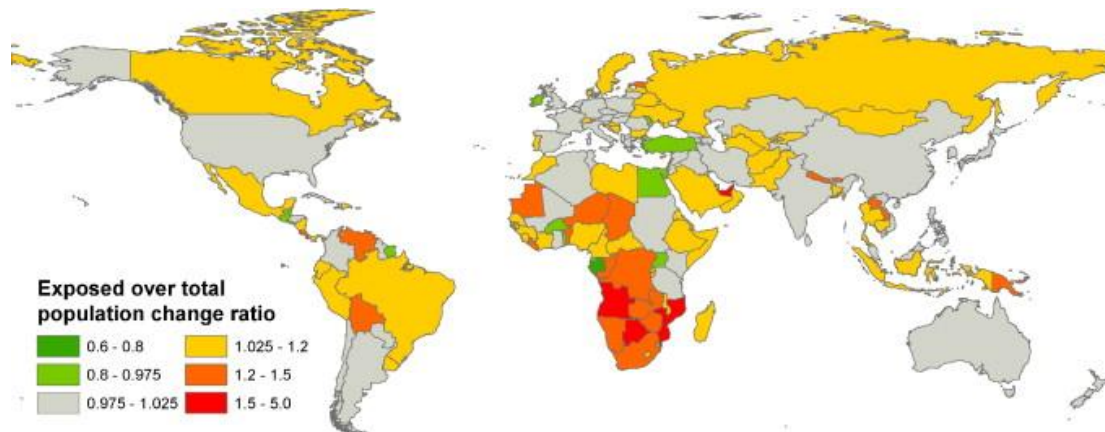


Figure 1.1: Map of relative changes in population exposed to 1 in 100 floods over changes in total population, 1970–2010 (Source: Jongman et al. (2012), *Global Environmental Change*).

They found that potential economic losses (Figure 1.2, b) were positively correlated with a global temperature increase, which is consistent with the increase in flood-exposed population reported earlier by Hirabayashi et al (2013). In contrast, the potential fatalities (Figure 1.2, a) decrease when the global temperature increased. This counterintuitive result was due to the effect of reduced vulnerability quantified in their model. However, when the effect of reduced vulnerability was not taken into consideration, both potential flood fatalities and economic losses were positively correlated with the temperature increase (black and grey lines in **Figure 1.2, a & b**).

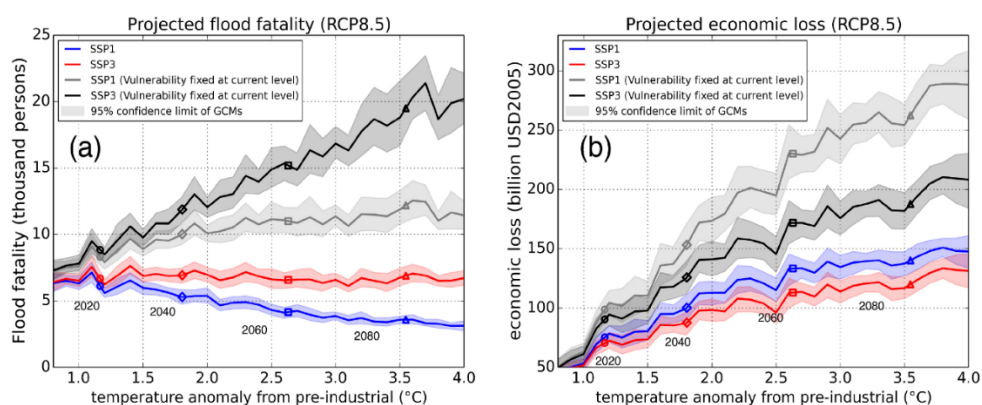


Figure 1.2: The relationship between the global temperature increase from the pre-industrial level (1850-1900) and potential flood consequences under the RCP8.5 scenario (Source: Kinoshita et al. (2018), *Environmental Research Letters*).

The increasing global losses demand effective and efficient risk-reducing strategies (Aerts et al., 2014, Brown et al., 2014), whose implementation should be based on an accurate understanding of the drivers of risk. This means it is of key importance to integrate both climate and anthropogenic drivers (Kim and Chung, 2014) into the flood management plans for identifying efficient strategies and policies.

1.2 Impacts of floods- ‘The Canadian story’

Floods are the most commonly occurring natural disaster in Canada and account for the largest share of recovery costs by any disaster on an annual basis (NRCan, 2018). Public Safety Canada (2017) reports that the number of flood events have increased between 1970 and 2015 as illustrated in **Figure 1.3**. Therefore, mapping and mitigating flood risks has become a key challenge to ensure resilience of the affected communities.

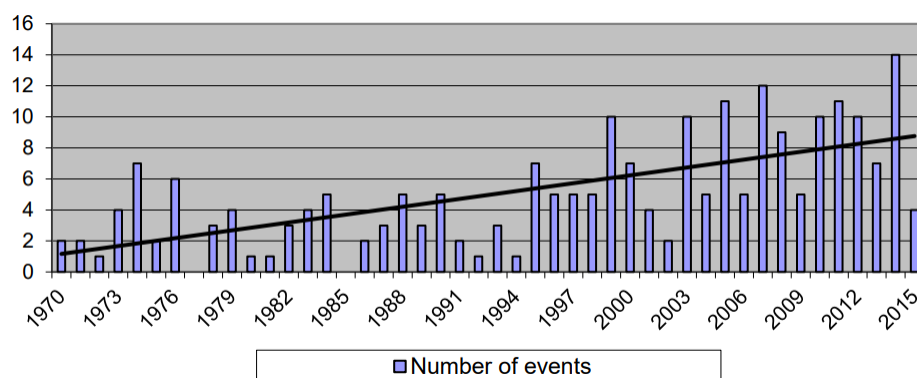


Figure 1.3: Trend in number of flooding events in Canada (Source: Public safety Canada, 2017)

Long back, the 1996 flood in Saguenay, Québec, was the first of its kind flood event which caused an economic damage exceeding CAD \$1 billion (Burn and Whitfield, 2016). A year later, the 1997 Red River flood in Manitoba was so severe, that it is termed as the “*flood of the century*” (Buckland and Rahman, 1999). In 2011, Manitoba was severely flooded by the Assiniboine River that resulted into an economic damage of CAD \$1.2 billion (Manitoba Infrastructure and Transportation, 2013). Flooding of the Bow and Elbow Rivers in southern Alberta in June 2013 became Alberta’s worst-ever natural disaster, with estimated costs of \$6 billion (Pomeroy et al., 2016). The researches on flooding over Canada are more widespread, due to evidence that the frequency, magnitude and economic damages from floods have risen in recent years as a result of increased human exposure to flood-prone areas as well as the

impacts of climate change (Simonovic and Li, 2003; Cunderlik and Simonovic, 2007; Samiran and Simonovic, 2012).

1.2.1 Status of floodplain mapping in Canada: Recent developments

In a large country like Canada, flood analysis and water resource management, in general, are tasks conducted at the provincial level; therefore, unified national-scale approaches to water related problems are uncommon. Flood management is inherently multi-faceted and involves a wide range of authorities and stakeholders, both within and outside of the government. Whereas the implementation of flood mitigation measures is mainly the responsibility of provincial/ territorial/local agencies, the federal government plays an important role in ensuring a broadly consistent national approach to flood mitigation. This involves establishing national floodplain mapping requirements, as well as basic criteria for geospatial data acquisition, management and dissemination. The federal government is committed to working with the provinces and territories on an ongoing basis through various federal-provincial-territorial forums related to Emergency Management, water resources and floodplain mapping, such as the Canadian Council on Geomatics (CCOG) and Senior Officials Responsible for Emergency Management (SOREM) to ensure Emergency Management policy/legislative coordination between all levels of government. Floodplain maps, which delineate the area inundated by a specified flood event, can serve a variety of uses, all of which are directed towards the reduction of flood risk.

Provincial and territorial governments are ultimately responsible for overseeing flood mitigation efforts within their jurisdictions. Although each province and territory manages flood risks separately, with the involvement of different departments and ministries, these efforts invariably involve collaboration with local municipalities or local water agencies to identify flood mitigation needs, establish priorities and implement initiatives, such as preparing and maintaining floodplain maps. In many cases, responsibility for such activities is delegated primarily to the municipalities and/or water agencies. At the municipal level, the identification of flood risks and implementation of flood mitigation measures takes place and local governments, working in conjunction with the provincial/territorial authorities, therefore play a central role in flood risk management. Municipal roles can include: water management, emergency management and continuity of service, land use planning/zoning regulation, critical infrastructure design and utility operation, public services, and ownership/operation/insurance of public assets, and climate change resilience and adaptation. Further, community outreach is

a critical element of flood risk management. It is critically important that individuals be aware of flood risks and the steps necessary to address them, both in terms of preparation and response. It is therefore essential that such information be made available to them by municipal authorities, particularly through the use of floodplain maps and other public outreach tools.

To address this topic, through consultation with provincial and territorial partners and key stakeholders, the federal government has developed a set of documents referred to as the Federal Floodplain mapping Guidelines Series (Public Safety Canada, 2019). The series covers all the components of the flood mitigation process, from flood hazard identification to the implementation of flood mitigation efforts. An outline of the proposed floodplain mapping framework is illustrated in **Figure 1.4**. More details are available at <https://www.publicsafety.gc.ca/cnt/mrgnc-mngmnt/dsstr-prvntn-mtgn/ndmp/fldpln-mppng-en.aspx>.

The framework consists of 4 main blocks (i) Flood Hazard Identification and Priority Setting, (ii) Hydrologic and Hydraulic Procedures for Flood Hazard Delineation, (iii) Geomatics Guidelines for Floodplain mapping, and, (iv) Risk-based Land-use Guide. Among them, the Floodplain mapping is a central component of the framework.

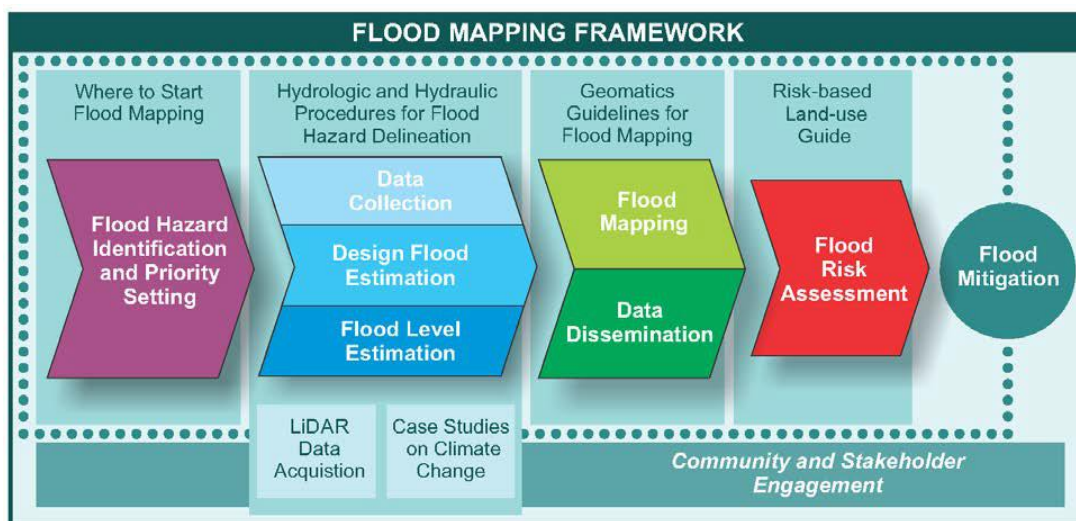


Figure 1.4: Floodplain Mapping Framework (Source: Federal Floodplain mapping Framework, Version 2.0 2018, Natural Resources Canada)

1.3 Challenges in floodplain mapping over large regions

Assessment of flood risk is a high priority topic, whose understanding is central for developing appropriate flood management strategies (Apel et al., 2009; Mohanty et al., 2020). Floodplain mapping refers to the delineation of flood extents and water elevations on a base map such as

topography, elevation, land-use etc. This typically consists of delineations on a map indicating the area that will be covered by water, or the elevation that water would reach during a specified flood event. Additional details may be displayed on the map, including: flow velocities, water depth, other risk parameters, and vulnerabilities. A representative floodplain map is shown in **Figure 1.5**.

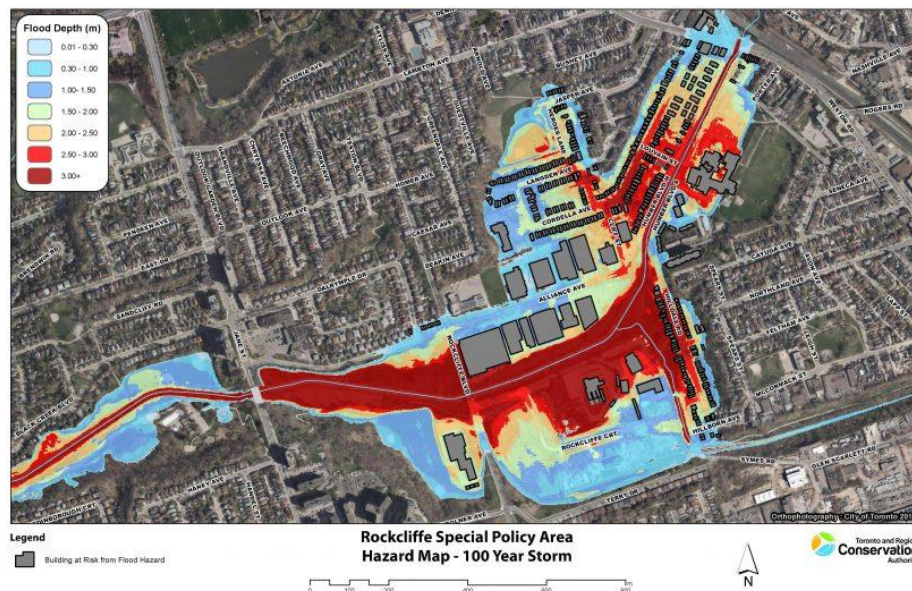


Figure 1.5: A representative illustration of floodplain map (Source: Haznet, 2019)

Most of the studies on floodplain mapping have limited their analysis to local and regional scales. However there was a growing need of extending it to larger scales of country and global level. (Ward et al., 2018). However, there were twin hurdles in accomplishing this goal: (i) huge computational power to perform inundation modeling (Jongman et al., 2012; Yamazaki et al., 2013) and, (ii) availability of global data sets to serve as model inputs (Woodhead et al., 2007). Over the years, a significant progress has been achieved in tackling these issues as detailed in the following sections.

1.3.1 Big data handling and large scale flood inundation mapping

To account for the difficulty linked with big-data handling and complex numerical simulations, last few years have seen an explosion of global flood inundation models (Hoch and Trigg, 2018). These models are tailor-made to present the hydrodynamics of flow by solving hydraulics- and physics-based equations. The flood hazard and risk maps are quantified from inundation outputs, which provide crucial information on the location, severity and degree of damage (Winsemius et al., 2016; Alfieri et al., 2017). Some widely used global flood models

and their sources are presented in **Table 1.1**. These models are now increasingly used for national flood hazard mapping, and flood forecasting in many countries.

Table 1.1: A list of widely used global flood models

Model name	Source
Catchment-Based Macro-scale Floodplain (CaMa-Flood) model	http://hydro.iis.u-tokyo.ac.jp/~yamadai/cama-flood/
Centro Internazionale in Monitoraggio Ambientale and United Nations Environment Program (CIMA-UNEP) model	https://www.preventionweb.net/organizations/8635
European Centre for Medium-Range Weather Forecasts (ECMWF) model	https://www.ecmwf.int/
Global Flood Risk (GLOFRIS) model	https://www.globalfloods.eu/
Joint Research Centre (JRC) model	https://ec.europa.eu/knowledge4policy/organisation/jrc-joint-research-centre_en
SSBN model (now known as Fathom Global Ltd)	https://www.fathom.global/
LIS-FLOOD	http://www.bristol.ac.uk/geography/research/hydrology/models/lisflood/

In general, these models: (i) estimate river flow for a given probability; and (ii) simulate water flow in the river channels and adjoining flood plains (Trigg et al., 2016). There are numerous studies which have utilized these sophisticated models for mapping floods spanning across country and global scales. Yamazaki et al. (2011) for the first time introduced CaMA-Flood, a global river routing model, to represent floodplain inundation dynamics at large scales. The model simulates flood flow behavior by establishing a relationship between the water storage, water level, and flooded area through parameterization of the sub-grid scale topographic parameters.

Pappenberger et al. (2012) proposed a cascading model by coupling ERA-Interim fed Hydrology Tiled ECMWF Scheme of Surface Exchanges over Land (HTESSEL) land surface model with the river routing algorithm within CaMa-Flood, to generate flood hazard maps at a resolution of 1km² for the entire globe. The global flood hazard maps were tested on 26 major

world river catchments by comparing with benchmark data sets developed by the 2011 Global Assessment Report on Disaster Risk Reduction. Hirabayashi et al. (2013) utilized CaMa-Flood to simulate flood inundation by utilizing discharge data from 11 Atmosphere-Ocean General Circulation Model (AOGCMs) from the Coupled Model Intercomparison Project (CMIP5) consortium. A similar study was later conducted by Koirala et al. (2014) with same AOGCMs, to identify agreement among them and evaluate the changes in global streamflow regimes at the end of the 21st century under RCP 4.5 and 8.5 scenarios. Willner et al. (2018) used CaMa-Flood to determine the historical and future flood risks across the globe by considering run-offs generated from a set of 10 hydrological models.

In a recent work, Gaur et al. (2018, 2019) used CaMa-Flood derived flood parameters to estimate the projected changes (2016-2100) in flood magnitudes and timings across Canada, and the implications on flow regulation infrastructure, respectively. Lim et al. (2018) considered daily runoff data from a baseline and 11 CMIP5 climate models to drive CaMa-Flood and derive global river water depths. Winsemius et al. (2013) built a comprehensive framework in GLOFRIS, to map flood hazard by using global forcing climate data from datasets (Climate Research Unit, CRU and ERA40 for historical and ECHAM5 and HadGEM2 for future); PCRaster Global Water Balance (PCR-GLOBWB) hydrologic model and dynamic routing procedure within DynRout. Ward et al., (2013) further downscaled the flood hazard extents to a finer scale of 1 km² to perform risk assessment based on GDP per capita data, population, and land-use maps. A similar framework was put-forward by Ward et al. (2017), to determine the accessing costs and benefits of structural protection measures in urban areas around the globe under various socio-economic development and climate change scenarios. A few other studies have utilized GLOFRIS to derive global river flood hazard maps showing inundation extent and depths (Muis et al., 2015; Haer et al., 2017, 2018).

A recent study by the European Commission's Joint Research Centre (EC-JRC) proposed a model cascade of distributed hydrological (LISFLOOD) and hydraulic model (LISFLOOD-ACC), driven by meteorological data (EFAS-Meteo dataset) for determining a 100-yr return period Pan European Floodplain map (Alfieri et al., 2014). Later, the historical flood hazard information derived from this study and future flood hazard information derived from Alfieri et al. (2015) were considered together along-side a socio-economic impact analysis in the form of depth-damage functions and a population density map, to estimate the potential damage and potential population affected by floods (Alfieri et al., 2015). In the same year, Sampson et al.,

(2015) developed a hydraulic engine based on sub-grid variant of LISFLOOD-FP to derive flood hazard maps at ~90 m resolution. The model results were found to perform well when validated with high-resolution government benchmark flood hazard maps over UK and Canada, and provided the least mean absolute error when aggregated at ~1 km resolution. Wing et al. (2017) adopted the same framework with United Nations Geological Survey National Elevation Dataset (USGS NED) data set to derive ~30 m resolution floodplain maps for the Contiguous United States (CONUS).

1.3.2 Publicly available datasets

The application of flood models over large regions have become easier with the release of publicly available global data sets. Remotely sensed topographic data such as Shuttle Radar Topography Mission (SRTM) and its improved version MERIT DEM (Yamazaki et al., 2017) and MERIT Hydro (Yamazaki et al., 2019), global river network details (Yamazaki et al., 2009; Wu et al., 2012); global hydrologic and meteorological data from reanalysis (Essou et al., 2016; Andreadis et al., 2017), GCMs (Jongman et al., 2015; Eisner et al., 2012); and tide data from global tide elevation (Wdowinski et al., 2016; Hunter et al., 2017), are now used extensively as inputs to global flood models. An exhaustive list of freely available datasets is shown in **Appendix A (Table A1)**.

1.4 Past efforts on floodplain mapping by utilising reanalysis datasets

The reanalysis datasets (term reanalysis stands for ‘retroactive analysis’) are produced by a weather forecasting models in the form of three-dimensional gridded data-sets at a global scale (Compo et al., 2011). They are used as an alternative dataset for regions where stations are sparsely distributed or non-existent (Dee et al., 2011; Sabarly et al., 2016). Reanalyses use a constant data assimilation scheme and numerical forecasting model, which ingests millions of available observations at a given time step over a given period (Bengtsson et al., 2004). Previous studies have evaluated whether meteorology derived from reanalysis data sets can reproduce the hydrology of river basins at multiple spatial and temporal scales (e.g., Essou et al., 2016). In addition, such studies within the context of flood modeling have either focused on river flow (e.g., Zsótér et al., 2016), have been performed at relatively coarse spatial scales (e.g., Emerton et al., 2017), or have only simulated flood return periods but not event time series (e.g., Ward et al., 2013). A few studies have compared a set of reanalyses data across the globe in their raw format (Hodges et al., 2003; Wang et al., 2006; Sabarly et al., 2016) or

obliquely by considering them as inputs to a hydrological model (Wu et al., 2012; Essou et al., 2016; Nkiaka et al., 2017). In general, studies on this topic have been based on a reduced number of watersheds, and no general consensus has been derived. A limited studies have considered reanalysis datasets as inputs to the flood models. Jongman et al. (2015) utilized precipitation from ERA-Interim reanalysis as input to PCR-GLOWB to simulate discharge and produce flood hazard maps for the entire globe. Dottori et al. (2016) considered ERA-Interim streamflow observations as input into GIoFAS- a probabilistic flood early warning system running at global scale comprising of HTESSEL land surface model and LISFLOOD hydrodynamic models, to produce global flood hazard maps at 30'' resolution. Later, Hirpa et al. (2016) compared the streamflow climatologies between ERA-Interim and Reforecast reanalyses product in a similar framework. The authors identified substantial dissimilarities in the flood thresholds, and also reported that ERA-Interim produced lower flood threshold exceedance probabilities than reforecast for several large rivers at short forecast lead times. Trigg et al. (2016) compared multi-probability flood hazard maps for Africa generated from six global flood models by using EU-WATCH, JRA-25, ERA-Interim, GIoFAS reanalyses datasets as specific model inputs. All of these studies demonstrated and have reported that on a global scale reanalyses can be extremely useful source of data. In a recent article, Andreadis et al. (2017) tried to find out if atmospheric reanalyses could be used to reproduce flooding over large scales. To answer this, the authors employed 20CRv2 reanalysis dataset into a coupled hydrologic/hydrodynamic model to quantify flood inundation and volume over Australia. The authors reported high correlations between the inundated areas and volume with observed benchmark dataset.

1.5 Past efforts on floodplain mapping by utilising global topographic datasets

Whereas, topographic datasets or Digital Elevation Models (DEMs) of higher resolution and accuracy are obtained through the commercial means like LiDAR, there are various other global sources which provide these data sets free of charge to end users, namely, Shuttle Radar Topography Mission (SRTM) and Advanced Spaceborne Thermal Emission and Reflection Radiometer (ASTER) digital elevation model from United States Geological Survey (USGS) (<https://earthexplorer.usgs.gov/>), and Advanced Land Observing Satellite (ALOS) (<http://www.eorc.jaxa.jp/ALOS/en/aw3d30/>). There are numerous other sources which have a global coverage and are commercially available on requests such as WORLD DEM (<http://www.intelligence-airbusds.com/en/4529-worlddem-reaching-new-heights>), AW3D

(aw3d.jp/en/), and Inter Map (<https://store.intermap.com/>). Some sources of DEM are country specific and hence are utilized locally for numerous applications. These sources include National Elevation Dataset (<https://lta.cr.usgs.gov/NED>) and GTOPO30 (<https://webgis.wr.usgs.gov/globalgis/gtopo30/>) for USA, CARTO DEM product (<https://data.gov.in/catalog/digital-elevation-model-dem-generated-cartosat-1-satellite-data-india>) for India, Canadian Digital Elevation Model (CDEM) (<http://geogratis.gc.ca/api/en/nrcan-rncan/ess-sst/c40acfba-c722-4be1-862e-146b80be738e.html>) for Canada, EU-DEM (<https://www.eea.europa.eu/data-and-maps/data/eu-dem>) for entire Europe, AHN-2 (http://gnss1.tudelft.nl/pub/ahn/ahn2_5/) for the Netherlands, NZ 8m DEM (<https://data.linz.govt.nz/layer/1768-nz-8m-digital-elevation-model-2012/>) for New Zealand and others.

In fact, many countries still lack the availability of national digital elevation models (DEMs) and hence have to rely on global datasets (Karlsson and Arnberg, 2011). There have been numerous studies, which utilized these global DEMs to conduct floodplain mapping and assessment for many parts, which were otherwise costly or unavailable at higher resolution. Wang et al. (2012) have concluded that SRTM and ASTER DEM can be beneficial in hydraulic modeling for data scarce conditions where high-resolution DEMs are not available. Patro et al. (2009) selected a delta region of Mahanadi River basin in India and demonstrated the usefulness of using SRTM (90m) to derive river cross-section for the use in hydraulic modelling in MIKE 11 and bathymetry for flood modelling using MIKE 21 and MIKE FLOOD (DHI, 2019). Paiva et al. (2011) demonstrated the use of SRTM DEM in a large-scale hydrologic model with a full 1-D hydrodynamic module to calculate flow propagation on a complex river network. The study was conducted on one of the major tributaries of the Amazon, the Purus River basin. Yan et al. (2013) also used the SRTM DEM as a geometric input to LISFLOOD-FP for flood inundation of Danube River under a data poor situation. Numerous other studies such as by Jung et al. (2011), Youssef and Pradhan (2011), Ho and Umitsu (2011) Bazgeer (2012), and Skakun et al. (2014) have used the SRTM DEM along with Landsat Thematic Mapper Plus (ETM+) in to derive floodplain maps. Tarekegn et al. (2010) used the ASTER data to create 15 m resolution DEM for two dimensional hydrodynamic flood modeling using the SOBEK flood model. They found that a representation of the river terrain largely affects the simulated flood characteristics. Also they concluded that the ASTER DEM is suitable for two dimensional hydrodynamic modeling purpose in cases when accurate high-resolution DEMs are unavailable. Gichamo et al. (2012) discussed an approach to generate

river cross-sections from ASTER DEM to simulate flooding on a part of the Tisza River, Hungary using the 1D river modeling tool HEC-RAS/GeoRAS (US Army Corps of Engineers, 2019). A vertical bias correction was carried out by comparison of elevation points with a high accuracy terrain model. Yamazaki et al. (2013) compared the ASTER images with the images of X band of Terra's Synthetic Aperture Radar (Terra SAR-X) for the flooded areas following the 2011 central Thailand flood. In another recent study, Sana Ullah et al. (2016) used ASTER 30 m DEM to model the flood inundation forecasting of the Kalpani River, Pakistan using the HEC-RAS (1D) and HEC-Geo RAS. Interestingly, inundation maps could not be prepared, because the HEC-GeoRAS failed to extract water surface grid from ASTER 30 m DEM. However, they found that the model can be used for flood risk management and as a decision support tool for the case study.

With all these relevant studies focussed on floodplain mapping, it is obvious that it is now much easier than before to perform large scale floodplain mapping. With the emergence of sophisticated flood models and publicly available datasets the process has become simpler. This technical report provides a detailed description on performing floodplain mapping over Canada by using freely available reanalysis datasets as inputs to the CaMa-Flood global flood model driven. **Chapter 2** provides a generic framework to perform floodplain mapping by utilising reanalyses datasets within flood model. This chapter also describes the structure of CaMa-Flood model in detail. **Chapter 3** provides a detailed methodology that has been adopted to perform flood inundation simulation over Canada starting from preparation of runoff inputs for CaMa-Flood using R programming language; use of high computing network SHARCNET (Shared Hierarchical Academic Network) for high speed runoff simulation by CaMa-Flood, and post-processing of results for further analysis.

Chapter 2 Proposed Floodplain Mapping Framework

A generic framework for performing large scale floodplain mapping by utilizing freely available datasets is illustrated in **Figure 2.1**. The framework consists of four major blocks, namely, (i) runoff observations (as input data set), (ii) CaMa-Flood model (for simulating floodplain mapping), and (iii) validation (for quantifying the model accuracy in capturing floodplains. The individual blocks are described in detail in the following sections.

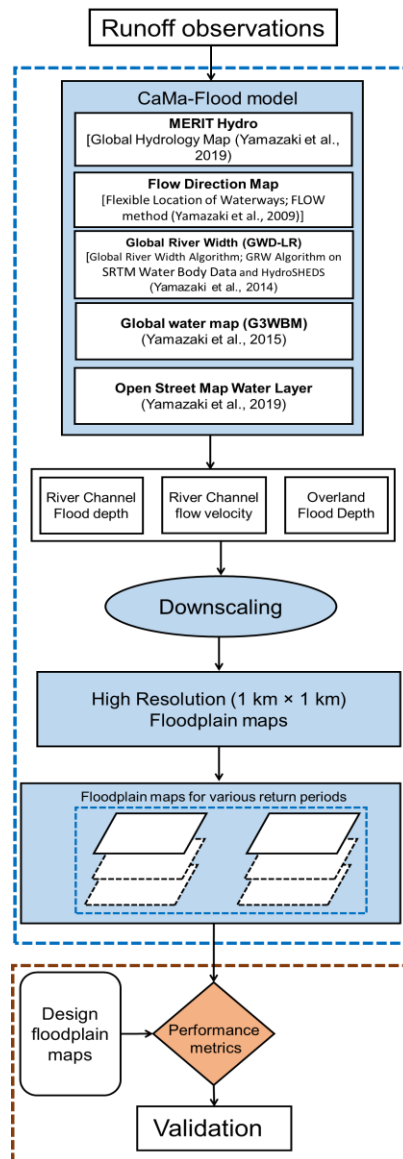


Figure 2.1: A generic framework of flood plain mapping using freely available datasets and global CaMa-Flood model

2.1 Run-off observations

Run-off observations can be obtained from a variety of sources as mentioned earlier in Section 1.3.2. Four globally available reanalysis datasets are utilized in the presented work and their detailed description and sources are provided in the **Appendix B**.

2.2 Catchment-based Macro-scale Floodplain (CaMA-Flood) Model

The CaMa-Flood model is a distributed global river routing model designed to simulate the hydrodynamics for large regions (Yamazaki et al., 2011; 2013; 2014). The global river networks are discretized to the hydrological units named unit-catchments for achieving efficient flow computation at a large scale. The water level and flooded area are derived from the water storage at each unit-catchment using the sub-grid topographic parameters of the river channel and floodplains. By adapting a grid-vector hybrid river network map, which maps one irregular-shaped unit-catchment to one grid-box, both, realistic parameterization of sub-grid topography and easy analysis of simulation results are achieved. The river discharge and flow velocity are calculated with the local inertial equation (Bates et al., 2010), along the river network map which prescribes the upstream-downstream relationship of unit-catchments. The time evolution of the water storage, the only one prognostic variable, is solved by the water balance equation which considers inflow from the upstream cells, outflow to the downstream cell and input from runoff forcing at each unit-catchment.

The major advantage of the CaMa-Flood simulations is the explicit representation of flood stage (water level and flooded area) in addition to river discharge. In addition to traditional model validation with gauged river discharge, it is possible to make a direct comparison between model simulations and satellite observations. The other advantage of the CaMa-Flood model is its high computational efficiency for the global river simulations. The complexity of the floodplain inundation processes is reasonably approximated to a diagnostic scheme at the scale of a unit-catchment by introducing the sub-grid topographic parameters. The cost of the prognostic computation of river discharge and water storage is optimized by implementing the local inertial equation (Bates et al., 2010) and the adaptive time step scheme (Hunter et al., 2005). The high computational efficiency of the CaMa-Flood model is beneficial for computationally demanding experiments such as ensemble/long-term simulations (Pappenberger et al., 2012; Hirabayashi et

al., 2013) and dynamic coupling between river routine and other hydrological schemes (Cohen et al., 2013).

The most recent model package (version 3.6.2) of CaMa-Flood is available by request at <http://hydro.iis.u-tokyo.ac.jp/~yamadai/cama-flood/>. In the recent version, the global river network maps are updated by seamless connection of Hydrological data and maps based on Shuttle Elevation Derivatives at multiple Scales (HydroSHEDS) (Lehner et al., 2006) and Global Drainage Basin Database (GDBD) (Yamazaki et al., 2011). A new Satellite-based river width from Global Width Database for Large Rivers (GWD-LR) (Yamazaki et al., 2014) and code for floodplain depth downscaling are also added. The flow direction is modified to keep a consistency with Global Width Database for Large Rivers. The grid-vector-hybrid river network map (the river network maps in previous versions) is updated in order to optimize the computational efficiency of simulations using the local inertial equation. The various components of the CaMa-Flood model are described in the following sections.

2.2.1 Components of the model

Flow Direction Map

The Flow direction map is represented by Flexible Location of Waterways (FLOW) method (Yamazaki et al, 2009), an upscaling algorithm which converts a high-resolution flow direction map into a coarse-resolution river network map. It also derives sub-grid-scale topographic parameters of the derived river network map, such as channel length, channel altitude, unit-catchment area, and floodplain elevation profile.

Global River Width (GWD-LR)

The Global Width Database for Large Rivers (GWD-LR) is developed by applying the algorithm to the SRTM Water Body Database and the HydroSHEDS flow direction map (Yamazaki et al., 2014). Both bank-to-bank river width and effective river width excluding islands are calculated for river channels between 60° S and 60° N. The effective river width of the GWD-LR is slightly narrower compared to the existing databases, but the relative difference is within 20% for most river channels. As the river width of the GWD-LR is calculated along the river channels of the

HydroSHEDS flow direction map, it is relatively straightforward to apply the GWD-LR to global- and continental-scale river modeling as well.

Global Water Map

Global 3 arc-second Water Body Map (G3WBM) is developed using an automated algorithm to process multi-temporal Landsat images from the Global Land Survey (GLS) database. Yamazaki et al. (2015) used 33,890 scenes from 4 GLS epochs in order to delineate a seamless water body map, without cloud and ice/snow gaps. Permanent water bodies were distinguished from temporal water-covered areas by calculating the frequency of water body existence from overlapping, multi-temporal, Landsat scenes. By analysing the frequency of water body existence at 3 arc-second resolution, the G3WBM separates river channels and floodplains more clearly than previous studies.

OSM Water Layer

OSM Water Layer is a global surface water data, generated by extracting surface water features from Open Street Map (Yamazaki et al., 2019). Both filtered OSM data (PBF format) and rasterized map (GeoTiff format) are available for use. For generation of rasterized map, surface water is classified into four categories, namely large Lake and River, Major River, Canal, and Minor Stream. The OSM water layer rasterized map is referenced to WGS 84. The data is available at 5 degree \times 5 degree tiles (6000 pixel \times 6000 pixel).

2.2.2 Model structure

The fine-resolution flow direction map from Global Drainage Basin Database (GDBD) (Masutomi et al., 2009) is available within the model. GDBD describes the downstream direction of each pixel at 1 km resolution in raster format. Each GDBD pixel is assumed to have only one downstream direction toward one of the eight neighboring pixels. The MERIT DEM (Yamazaki et al., 2019) is employed as an input DEM for the FLOW method. The MERIT DEM is one of the most accurate DEMs covering almost the entire globe and has a comparable spatial resolution to GDBD. Because of the difference in geometric projections between GDBD and MERIT DEM, MERIT DEM was spatially interpolated to create a surface elevation map with the same grid coordinate as GDBD.

To remove the inland sinks, which interfered with flow going downstream in the surface elevation map, the elevation profile along river channels of GDBD was also smoothed.

Unit catchment and sub-grid topography

The parameters and variables used in CaMa-Flood are listed in **Table 2.1**. Each grid point over the domain has a river channel reservoir and a floodplain reservoir, as illustrated in **Figure 2.2**. The floodplain reservoir (**Figure 2.2, a**) consists of the unit catchment of the river channel (**Figure 2.2, b**) for each grid point, so that some areas that might never be flooded are also included in the floodplain reservoir. River channel and floodplain are treated as continuous reservoirs in that water spilling from the river channel is stored in the floodplain. This idea of assuming polygonal storages for river channels and floodplains is adapted in order to represent the realistic relationship between water storage and stage.

A river channel reservoir has three parameters: channel length, L , channel width, W , and bank height, B . On the other hand, a floodplain reservoir has a parameter for unit catchment area, A_c , and a floodplain elevation profile, $D_f = D(A_f)$, which describes floodplain water depth, D_f , as a function of flooded area, A_f . For simplification, D_f is given as an increasing function of A_f (**Figure 2, c**), so that no local depression is assumed in the floodplain elevation profile. This simplification is based on the assumption that inundation always occurs from lower to higher places within a unit catchment. Note that all topographic depressions, including permanent lakes and wetlands, are treated as “floodplain storages” within the framework of CaMa-Flood model.

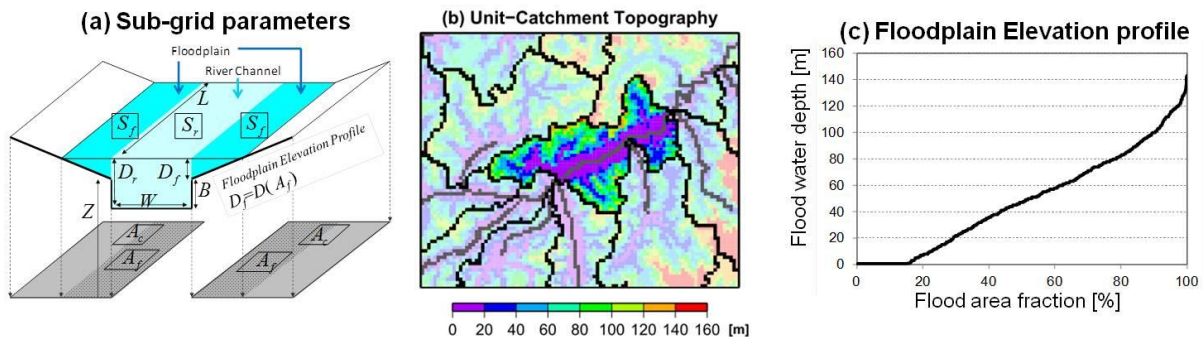


Figure 2.2: (a) Illustration of a river channel reservoir and a floodplain reservoir defined in each grid

Table 2.1: Parameters and variables in CaMa-Flood model.

Symbol	Name	Unit
Parameters		
L	channel length	m
W	channel width	m
B	bank height	m
Z	surface altitude	m
X	distance to downstream cell	m
A_c	unit catchment area	m ²
n	Manning's roughness coefficient	m ^{-1/3} s
Variables		
S	total water storage, $S_r + S_f$	m ³
S_r	river channel water storage	m ³
S_f	floodplain water storage	m ³
D_r	river water depth	m
D_f	floodplain water depth	m
H	effective river depth	m
A_f	flooded area	m ²
R	runoff from land surface model	m/s
Q	discharge	m ³ /s
R_{up}	maximum 30 day upstream runoff	m ³ /s
v	river flow velocity	m/s
i_o	riverbed slope	
i_{sfc}	water surface slope	
i_f	friction slope	

River channel water storage, S_r , floodplain water storage, S_f , river channel water depth, D_r , floodplain water depth, D_f , and flooded area, A_f , are diagnosed from the total water storage of a grid point, S , by solving simultaneous equations (2.1 to 2.5) or (2.6 to 2.10) below. One of the simultaneous equations (2.1 to 2.5) or (2.6 to 2.10) is chosen by comparing the total water storage, S , against the flood initiation storage, $S_{ini} = BWL$, where B is bank height, W is channel width, and L is channel length.

For cases in which total water storage, S , is less or equal to the flood initiation storage, S_{ini} .

$$S_r = S \quad (2.1)$$

$$D_r = \frac{S_r}{WL} \quad (2.2)$$

$$S_f = 0 \quad (2.3)$$

$$D_f = 0 \quad (2.4)$$

$$A_f = 0 \quad (2.5)$$

For cases in which total water storage, S , is greater than the flood initiation storage,

$$S_r = S - S_f \quad (2.6)$$

$$D_r = \frac{S_r}{WL} \quad (2.7)$$

$$S_f = \int_0^{A_f} (D_f - D(A)) dA \quad (2.8)$$

$$D_f = D_r - B \quad (2.9)$$

$$A_f = D^{-1}(D_f) \quad (2.10)$$

The equation $D_f = D_r - B$ in (2.9) means that the water surface elevations of the river channel and the floodplain are the same. This equation is based on the assumption that water mass is instantaneously exchanged between the channel and the floodplain to balance the water surface elevations of the two reservoirs. The function $D^{-1}(D_f)$, which is the inverse function of $D(A_f)$, describes flooded area, A_f , as a function of floodplain water depth, D_f (Figure 2, c). The simultaneous equations (2.6 to 2.10) are solvable because the elevation profile function, $D_f = D(A_f)$, was assumed to be an increasing function.

River network map & discharge calculation

The water exchange between the unit catchments occurs along the river network map. The river discharge is calculated with the local inertial equation (Bates et al., 2010). The local inertial equation is derived by neglecting the second term (advection) of the St. Venant's momentum expression as mentioned in equation 2.11.

$$\frac{\partial Q}{\partial t} + \frac{\partial}{\partial x} \left[\frac{Q^2}{A} \right] + \frac{gA \partial(h+z)}{\partial x} + \frac{gn^2 Q^2}{R^{4/3} A} = 0 \quad (2.11)$$

The first, second, third and fourth terms represent the local acceleration, advection, water slope, and friction slope, respectively. The explicit form of the local inertial equation (2.12) is used in the CaMa-Flood model.

$$Q^{t+\Delta} = \frac{Q^t - \Delta t g A S}{\left(1 + \frac{\Delta t g n^2 |Q^t|}{R^{4/3} A}\right)} \quad (2.12)$$

The negative river discharge, which may occur in the calculation by the local inertial equation and the diffusive wave equation, represents the backward water flow from the downstream grid cell towards the current grid cell.

Storage change and flood plain flow

The storage change at each grid cell from the time t to $t+\Delta t$ is calculated by the mass conservation as described in equation 2.13:

$$S_i^{t+\Delta t} = S_i^t + \sum_k^{upstream} Q_k^t \Delta t - Q_i^t \Delta t + A c_i R_i^t \Delta t \quad (2.13)$$

where S_i^t and $S_i^{t+\Delta t}$ represent the water storage of grid i at the time t and $t+\Delta t$, Q_i^t represents the river discharge outflow from grid i at time t , Q_k^t represents the river discharge inflow from the upstream grid k , $A c_i$ is the unit catchment area of grid i , and R_i^t represents the input runoff to the grid i . Floodplain discharge is also calculated by the local inertial equation (2.13). The flow area A is calculated by dividing floodplain storage by channel length. The flow depth h is given by the floodplain depth.

2.3 Validation of floodplain maps

Depending on the objective of model simulations, the floodplain maps can be validated by comparing with either benchmark floodplain maps available with various river organisations, or satellite observations. Most of the benchmark floodplain maps are available upon requests, while satellite observations are available publicly, for instance at https://www.eodms-sgdot.nrcan-rncan.gc.ca/index_en.jsp (for Canada coverage) and <https://www.gdacs.org/flooddetection/> (for global coverage). Most of these maps are available as GeoTIFF, and hence can be opened using any GIS tool. Different performance metrics can be considered to determine the validation between

the two floodplain maps. A few widely used metrics are, Hit Rate, False Alarm Ratio, Critical Success Index, and Error Bias.

The *Hit Rate (H)*, sometimes referred to as the probability of detection, is a simple measure that indicates how well the model replicates the benchmark data without penalizing for overprediction. It is expressed as in equation 2.14

$$H = \frac{A_m \cap A_b}{A_b} \quad (2.14)$$

where A_m is the modeled inundated area and A_b in the benchmark inundated area. H ranges from 0 to 1, with a score of 1 indicating that all wet cells in the benchmark data are wet in the model data.

The *False Alarm Ratio (F)* is a measure of model overprediction (i.e., “false alarms”) as expressed in equation 2.15:

$$F = \frac{A_m / A_b}{(A_m \cap A_b + A_m / A_b)} \quad (2.15)$$

A value of 0 indicates no false alarms, while 1 indicates false alarms.

The *Critical Success Index (C)* combines H and F into a score that penalizes for both underprediction and overprediction. It is expressed as,

$$C = \frac{A_m \cap A_b}{A_m \cup A_b} \quad (2.16)$$

A value of 0 indicates no match between model and benchmark, while 1 indicates perfect match between benchmark and model.

An *Error Bias* can be expressed as

$$B = \frac{A_m / A_b}{A_b / A_m} \quad (2.17)$$

Chapter 3 Floodplain Mapping Methodology

A detailed methodology for producing flood inundation maps by utilizing the global datasets with the CaMa-Flood model is presented here. The complete methodology can be sub-divided into five steps namely: (i) extraction of runoff from reanalyses products, (ii) preparation of input files for CaMa-Flood model, (iii) model simulation with high computing system, (iv) processing generated outputs, and (v) conversion of outputs to GeoTIFF format for output visualization in a GIS environment. Each step is detailed in the following paragraphs.

3.1 Extraction of runoff data from reanalysis datasets

The runoff datasets are usually available in a NetCDF (.nc) format in the parent websites as described in Table A.1. These files are accessed by using R statistical and programming language. The data can be extracted for the area of interest (AoI) and saved in a numeric format.

3.2 Preparation of input files for CaMa-Flood model

At first, the extracted runoff datasets for the AoI are interpolated to $1^\circ \times 1^\circ$ resolution on grids between 180°W to 180°E and from 90°N to 90°S as input data for the CaMa-Flood model. In the next step, the data is interpolated using Inverse Distance Squared method for filling the missing values, if any. In this method, the data at a particular grid point is considered to be inversely proportional to the square of distance from the nearest model grid point (equation 2.18). The distance of point of interpolation is found out from four nearest reanalysis data grid points surrounding it. The interpolated value at the particular location (v_i) is calculated by finding the sum of weighted means of runoff data at all four grid points (v_j) using equation 2.19.

$$w_j = \frac{1/d_j^2}{1/d_1^2 + 1/d_2^2 + 1/d_3^2 + 1/d_4^2} \quad (2.18)$$

$$w_j = \sum_{j=1}^4 w_j \times v_j(t) \quad (2.19)$$

where d_1, d_2, d_3 and d_4 are the distances of the location of interpolation from four nearest grid points and w_j is the weight calculated for j^{th} grid point.

3.3 Model simulation

The directories present in the CaMa-Flood package are tabulated in **Table 3.1**. The CaMa-Flood model simulations are performed using the SHARCNET supercomputing system (<https://www.sharcnet.ca/>). At first, one can Download and install WinSCP and PuTTY.exe (as shown **Figures 3.1 and 3.2**) software packages.

Table 3.1: List of directories in the CaMa-Flood package (version 3.6.2).

Directories	Purpose
\$ (CaMa-Flood)/	Main Directory
adm/	Administration Directory, contains Mkinclude
gosh/	Shell Scripts Directory, for executing simulations
src/	Main Source Code Directory
lib/	Library Code Directory
mod/	Module Code Directory
map/	Map Directory, contains river network maps
inp/	Input Directory, contains a sample input data
out/	Output Directory, contains some programs for data processing
etc/	Various programs for analysis, visualization, etc.

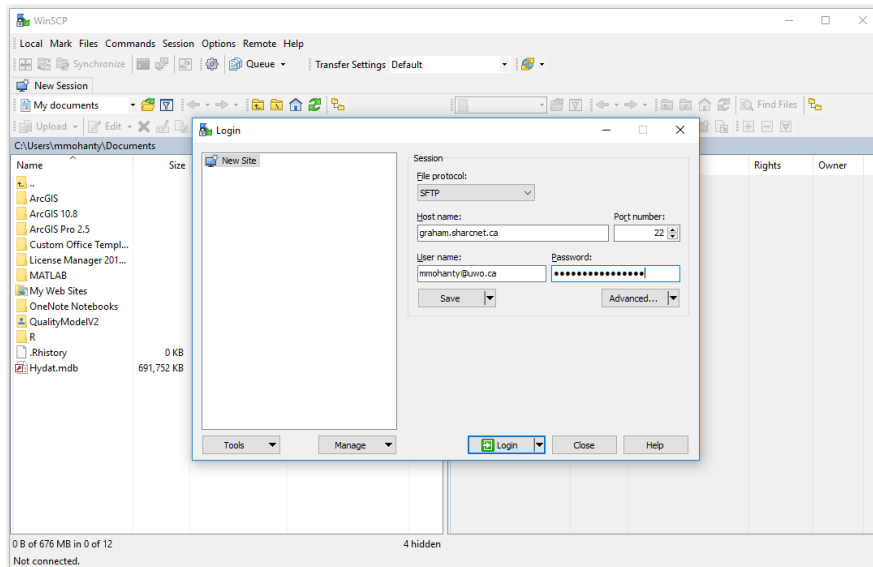


Figure 3.1: WinSCP window login window

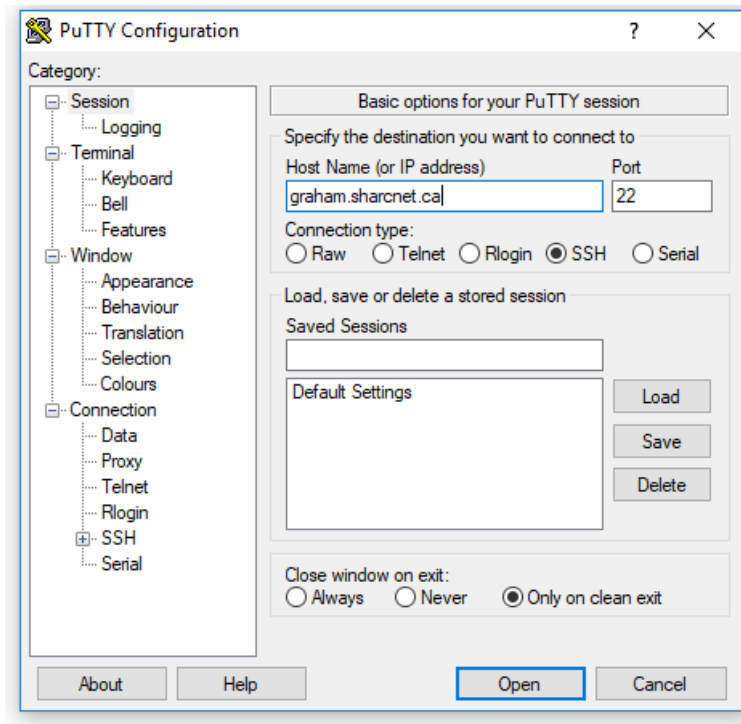


Figure 3.2: PuTTY configuration window

Once done, the modules and paths can be set by running the command as provided in **Figures 3.3 and 3.4**. By doing so, SHARCNET will be able to find “gcc” and “ifort” compiler automatically. This process should be accomplished each time the user log into SHARCNET. CaMa-flood can utilize multiple cores for model simulations. This can be set-up with the code presented in **Figure 3.5**.

```
module unload intel mkl openmpi
module load intel/15.0.6
export
LD_LIBRARY_PATH=/opt/sharcnet/testing/netcdf/4.3.2/lib:/opt/sharcnet/netcdf/4.3.2/lib:$LD_LIBRARY_PATH
```

Figure 3.3: R code for Connecting to SHARCNET

```
RM = /bin/rm -f
CP = /bin/cp
# DMPI: activate when using MPI
# DCDF: activate when using netCDF
# DEND: activate when endian conversion is needed
#DMPI=-DUseMPI
DCDF=-DUseCDF
#DEND=-DConvEnd
```

```

CFLAGS=$(DMPI) $(DCDF) $(DEND)

### gfortran ###
INC = -I/opt/sharcnet/netcdf/4.3.2/include -I/opt/sharcnet/testing/netcdf/4.3.2/include
LIB = -L/opt/sharcnet/netcdf/4.3.2/lib -L/opt/sharcnet/testing/netcdf/4.3.2/lib -lnetcdff
#-lnetcdff
CPP = gcc -E $(CFLAGS)
FC = ifort -openmp
LFLAGS =
FFLAGS = -O3 -warn all -assume byterecl -heap-arrays
# FFLAGS = -O3 -Wall -g -ffpe-trap=invalid,zero,overflow,underflow -fbounds-check -
mcmmodel=medium -fbacktrace -fdump-core
### ifort ### #INC = -I/usr/local/include
#LIB = -L/usr/local/lib -lnetcdf
#CPP = /usr/bin/gcc -E $(CFLAGS)
#FC = ifort -openmp
#FC = ifort #LFLAGS =
#FFLAGS = -O3 -warn all -assume byterecl -heap-arrays
# FFLAGS = -O3 -Wall -g -ffpe-trap=invalid,zero,overflow,underflow -fbounds-check -
mcmmodel=medium -fbacktrace -fdump-core
### ifort
### #INC = -I/usr/local/include
#LIB = -L/usr/local/lib -lnetcdf
#CPP = /usr/bin/gcc -E $(CFLAGS)
#FC = ifort -openmp
#FC = ifort
#LFLAGS =
#FFLAGS = -O3 -warn all -assume byterecl -heap-arrays
### MPI ###
#INC = -I/opt/local/include
#LIB = -L/opt/local/lib -lnetcdf
#FC = mpif90
#CPP = /usr/local/bin/gcc -E $(CFLAGS)
#LFLAGS =
#FFLAGS = -O3 -Wall

```

Figure 3.4: Commands to set the modules and paths in Mkinclude file

```

sqsub -q threaded -n 24 -r 4h --mpp=16g -o outputfile.txt bash global_15min.sh

```

Figure 3.5: Code to submit the jobs in PuTTY and run the code on SHARCNET

3.4 Outputs processing

A set of 14 flood water related channel and overland outputs are generated by the CaMa-Flood model simulations as shown in **Table 3.2**. The simulated model outputs are generated in the binary format (.bin), and require a conversion to numeric values for interpretation and further analysis. However, since the objective of the work presented in this report is to derive floodplain maps, we consider the Floodplain Water Depth, River Water Depth, and Flood Area for further analysis.

Table 3.2: List of floodwater related outputs generated from CaMa-flood simulation

File name	Variable	Symbol	Description	Unit	Format
rivoutYYYYY.bin	rivout	Q_r	River Discharge	m ³ /s	Real
rivstoYYYYY.bin	rivsto	S_r	River Water Storage	m ³	Real
rivdphYYYYY.bin	rivdph	D_r	River Water Depth	m	Real
rivelYYYYY.bin	rivel	V	River Flow Velocity	m/s	Real
fldoutYYYYY.bin	flddph	Q_f	Floodplain Flow	m ³ /s	Real
fldstoYYYYY.bin	fldsto	S_f	Floodplain Water Storage	m ³	Real
flddphYYYYY.bin	flddph	D_f	Floodplain Water Depth	m	Real
fldareYYYYY.bin	fldare	A_f	Flood Area	m ²	Real
fldfrcYYYYY.bin	fldfrc	F_f	Flood Fraction	m ² / m ²	Real
sfcelvYYYYY.bin	sfcelv	WSE	Water Surface Elevation	m	Real
outflwYYYYY.bin	outflw	Q_{all}	Total Discharge ($Q_r + Q_f$)	m ³ /s	Real
storgeYYYYY.bin	storge	S_{all}	Total Storage ($S_r + S_f$)	m ³	Real
pthoutYYYYY.bin	pthout	Q_p	Net bifurcation flow from grid (i_x, i_y)	m ³ /s	Real
pthflwYYYYY.pth	pthflw	--	Flow of bifurcation channel ($ipth, ilev$)	m ³ /s	Real

3.5 Conversion of outputs to GeoTIFF format

After converting the requisite outputs to a numeric format, they can be converted to a GeoTIFF (Raster), for visualizing in a GIS environment. Visualizing the results in a GIS environment helps in preparation of maps, as well as light statistical analysis without any demanding computations.

3.6 Validation of floodplain maps

The floodplain maps can be validated with the benchmark floodplain maps through a statistical package or GIS platform. In this study, we used ArcGIS 10.6 to perform statistical analysis and visualize them in the form of maps. ArcGIS can be obtained from

<https://www.arcgis.com/index.html>. It should be made sure that the spatial analyst tool is installed and supported by the system to perform the analysis. The **Figure 3.6** shows an overview of the ArcGIS administrator to make sure the relevant software components are installed.

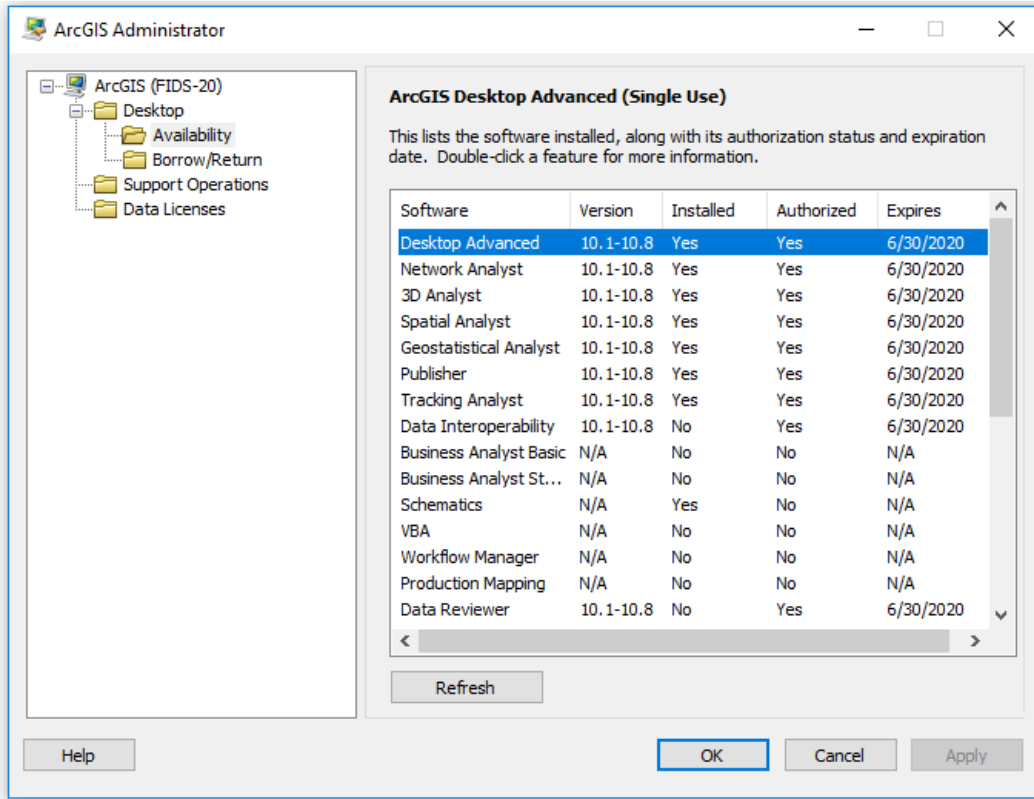


Figure 3.6: ArcGIS 10.6 administrator

Chapter 4 Sample model simulation and analysis

This section describes a more detailed description to obtain high resolution floodplain maps by considering NARR reanalysis data as input to the CaMa-Flood model. The NARR runoff data is available from 1979 to 2020 at a temporal resolution of 3-hours. A set of R codes are used to access the runoff files, extract and process the runoff to be used as inputs to the CaMa-Flood, and perform post-processing on the outputs. The step-wise procedure includes: (i) downloading reanalysis data, (ii) accessing reanalysis data, (ii) extracting runoff values for the AoI, (iii) converting runoff from numerical to binary format, (iv) model run in SHARCNET, and (v) conversion to requisite format for possible impact analyses.

4.1 Downloading NARR reanalysis

The 3-hourly NARR reanalysis runoff data for a duration from 1979 to 2020 is available at <ftp://ftp.cdc.noaa.gov/Datasets/NARR/monolevel/> as shown in **Figure 4.1**. In the website, the runoff data is available at various temporal resolutions as shown in **Figure 4.1 (a)**. By clicking on the 3-hourly accumulation runoff, it directs directly to the download page as shown in **Figure 4.1 (b)**. Search for keywords ‘*ssrun*’ corresponding to 3-hourly runoff data as shown in **Figure 4.1 (c)**.

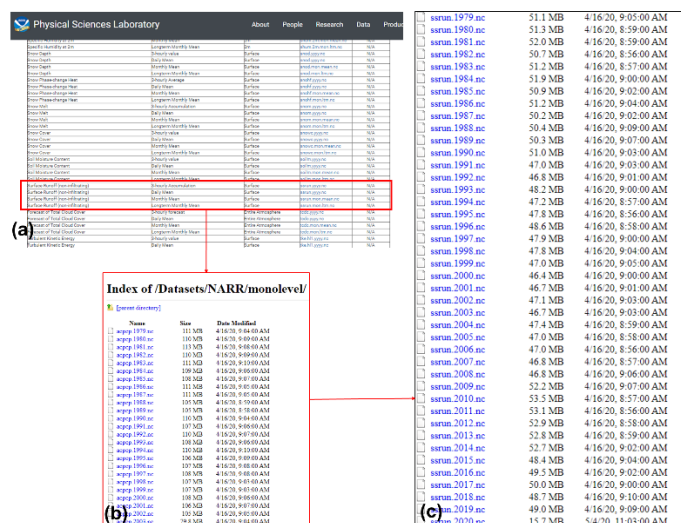


Figure 4.1: NARR runoff data: (a) data availability at <ftp://ftp.cdc.noaa.gov/Datasets/NARR/monolevel/>; (b) Index of datasets; and (c) runoff files from 1979 to 2020

This data is available in NetCDF format. NetCDF is a set of self-describing software libraries, machine-independent data formats that support the creation, access, and sharing of array-oriented scientific data. NetCDF files also contain dimensions, which describe the extent of the variables arrays. Files not only contain the "data" but also a description of the variables, the creation history, and any other important attributes of the data set. Version 4 of the NetCDF library stores data in HDF5 format files; while earlier versions store data in a custom format.

4.2 Accessing reanalysis data

The NARR runoff files in NetCDF file format are accessed in R using the function provided in **Figures 4.2 to 4.4**. The runoff files are used to extract longitude, latitude information and time indices are extracted from the '.nc' file, and interpolation is performed to read the '.nc' runoff files. Some additional packages like *ncdf4*, *lubridate*, *ggplot2*, *reshape2* along with *ncdf4*, are used for performing various other tasks. For example, *ncdf4* is used to access '.nc' GCM files, *lubridate* is used for dates related functions, *ggplot2* and *reshape2* for plotting purposes, etc.

```

1 library(ncdf4)
2 library(lubridate)           #Packages useful for the Reanalysis data analysis .
3 library(ggplot2)
4 library(reshape2)
5 library(rgdal)
6
7
8 ncfFile="w:/Research work/CaMaFlood Package_Yamazaki/Main Package CaMa-Flood_v3.6.2_20140909.tar/CaMa-Flood_v3.6.2_20140909/inp/ELSE_GPCC/runoff_nc/runoff1990.nc"
9
10 #stationlist represents coordinates where we need to interpolate the data...
11 #stationlist=data.frame(Lon=c(-100,-90,-80,-120,-150,-130,-120),Lat=c(50,60,70,85,75,65,55))
12 #Longitudes as Latitudes where we need to interpolate the data which is called stationlist.
13 ncfFiles=list.files("c:/Research work/Reanalysis_Dailymean_Runoff_NARR",pattern="ssrun.*.nc",full.names=T)
14 #reading the main NARR Reanalysis file for the duration 1979-2010.
15 varname="ssrun" #variable name=Surface Runoff
16 #sub1 is the main file for interpolation..sub2 is for finding nearest points and their weights.
17 stationlist=data.frame(Lon=rep(seq(-180,179,by=1),times=180),Lat=rep(seq(90,-89,by=-1),each=360))
18 write.csv(stationlist,"c:/Research work/Reanalysis_Dailymean_Runoff_NARR/Results_NARR/stationlist for CaMaFlood.csv")
19
20 #Importing canada shapefile:
21 can.shp <- readOGR("c:/Research work/Reanalysis_Dailymean_Runoff_NARR/Results_NARR/CAN_adm0.shp", "CAN_adm0")
22 print(proj4string(can.shp))
23
24 #Convert stationlist to sp object.
25 coordinates(stationlist) <- c("Lon", "Lat")
26 #confirm that projection is same for both points and shapefile
27 proj4string(stationlist) <- proj4string(can.shp)
28
29 # combine is.na() with over() to do the containment test; note that we
30 # need to "demote" can.shp to a SpatialPolygons object first
31 inside.can <- data.frame(stationlist[!is.na(over(stationlist, as(can.shp, "SpatialPolygons"))),])
32
33 #points located within Canada...
34 write.csv(inside.can,"c:/Research work/Reanalysis_Dailymean_Runoff_NARR/Results_NARR/stationlist for CaMaFlood model_points located within Canada.csv")

```

Figure 4.2: R code for accessing and extracting NARR NetCDF reanalysis files

```

1 Interpolate=function(ncfile,stationlist,date_ser)
2
3 nc_file=nc_open(ncfile)
4 #opened file is used to extract longitude and latitude information:
5 lon=ncvar_get(nc_file,"lon")
6 lat=ncvar_get(nc_file,"lat")
7
8 #Longitudes are adjusted to accommodate for a 0-360 scale in lon in NCEP data:
9 if(max(lon)>180)
10   lon[which(lon>180)]=lon[which(lon>180)]-360
11
12 #Preparing the coordinate matrix:
13 coord_mat=data.frame(lon=rep(lon,length(lat)),lat=rep(lat,each=length(lon)))
14
15 #Performing nearest squared distance interpolation:
16 d=do.call(cbind,lapply(1:nrow(stationlist),function(x){(stationlist$lon[x]-coord_mat$lon)^2+(stationlist$lat[x]-coord_mat$lat)^2}))
17 close_ind=do.call(cbind,lapply(1:ncol(d),function(x){order(d[,x])[1:4]}))
18 w=close=do.call(cbind,lapply(1:ncol(close_ind),function(x){1/d[close_ind[,x]}))
19
20 #find out which days should be extracted:
21 #Extract the reference date info from the nc file.
22 ref_date=as.date(strsplit(strsplit(nc_file$dim[which(names(nc_file$dim)
23   == "time")])$units,"since")[[1]][2],"00:00:0.0")[[1]][1]
24 if(grep("days",nc_file$dim[which(names(nc_file$dim) == "time")])$units=="")
25   {
26   #if leap years are considered.
27   data_dates=ref_date+ceiling(nc_file$dim[which(names(nc_file$dim) == "time")])$vals)
28
29   #if leap years are not considered.
30   if(ceiling(nc_file$dim$timeslen)%365==0)
31   {
32   all_dates=seq(from=ref_date,
33     to=as.date(paste((year(ref_date)+ceiling(nc_file$dim[which(names(nc_file$dim) == "time")])$vals(nc_file$dim$timeslen)/365)),"-12-31",sep=""),by="day")
34
35   leap_dates=intersect(which(month(all_dates)==2),which(day(all_dates)==29))
36
37   noleap_dates=all_dates
38   if(length(leap_dates)>0)
39     noleap_dates=all_dates[-leap_dates]
40
41   data_dates=noleap_dates[ceiling(nc_file$dim[which(names(nc_file$dim) == "time")])$vals[1]:ceiling(nc_file$dim[which(names(nc_file$dim) == "time")])$vals(nc_file$dim$timeslen)]
42
43 }
44
45 #if 360 days are considered in a year.
46 if((ceiling(nc_file$dim$timeslen)%360==0) &&
47   ceiling(nc_file$dim$timeslen)%365!=0)
48 {
49   year_ser=rep(year(ref_date):(year(ref_date)+ceiling(nc_file$dim[which(names(nc_file$dim)
50     == "time")])$vals(nc_file$dim$timeslen)/360)),each=360)
51
52   month_ser=rep(rep(1:12,(length(year_ser)/360)),each=30)
53   day_ser=rep(1:30,(12*length(year_ser)/360))
54   all_dates=as.date(sapply(1:length(year_ser),function(x){paste(year_ser[x],"-",month_ser[x],"-",
55     day_ser[x],sep="")}))
56   all_dates=all_dates[which(all_dates==ref_date):length(all_dates)]
57   data_dates=all_dates[ceiling(nc_file$dim[which(names(nc_file$dim) == "time")])$vals[1]:ceiling(nc_file$dim[which(names(nc_file$dim) == "time")])$vals(nc_file$dim$timeslen)]
58 }
59 #find out which time indices are to be extracted from the ncfile.
60 ind_dataext=which(as.character(data_dates) %in% as.character(date_ser))
61
62 if(length(ind_dataext)!=0)
63 {
64 #Extract dataset for extracted time and location indices:
65 #First extracting data at 4 nearest grids for each station and combining them as a list.
66 #In the output, each list component represents a station, columns within the list represent number of days and rows
67
68 #nearest neighbour datasets.
69 data_int=do.call(rbind,lapply(1:length(ind_dataext),function(x){apply(matrix(ncvar_get(nc_file,varid=names(nc_file$var)[4],
70

```

Figure 4.3: R code for interpolation

```

43 }
44
45 #if 360 days are considered in a year.
46 if((ceiling(nc_file$dim$timeslen)%360==0) &&
47   ceiling(nc_file$dim$timeslen)%365!=0)
48 {
49   year_ser=rep(year(ref_date):(year(ref_date)+ceiling(nc_file$dim[which(names(nc_file$dim)
50     == "time")])$vals(nc_file$dim$timeslen)/360)),each=360)
51
52   month_ser=rep(rep(1:12,(length(year_ser)/360)),each=30)
53   day_ser=rep(1:30,(12*length(year_ser)/360))
54   all_dates=as.date(sapply(1:length(year_ser),function(x){paste(year_ser[x],"-",month_ser[x],"-",
55     day_ser[x],sep="")}))
56   all_dates=all_dates[which(all_dates==ref_date):length(all_dates)]
57   data_dates=all_dates[ceiling(nc_file$dim[which(names(nc_file$dim) == "time")])$vals[1]:ceiling(nc_file$dim[which(names(nc_file$dim) == "time")])$vals(nc_file$dim$timeslen)]
58 }
59 #find out which time indices are to be extracted from the ncfile.
60 ind_dataext=which(as.character(data_dates) %in% as.character(date_ser))
61
62 if(length(ind_dataext)!=0)
63 {
64 #Extract dataset for extracted time and location indices:
65 #First extracting data at 4 nearest grids for each station and combining them as a list.
66 #In the output, each list component represents a station, columns within the list represent number of days and rows
67
68 #nearest neighbour datasets.
69 data_int=do.call(rbind,lapply(1:length(ind_dataext),function(x){apply(matrix(ncvar_get(nc_file,varid=names(nc_file$var)[4],
70

```

Figure 4.4: R code for interpolation (contd...)

4.3 Extracting runoff values for AoI

Once the reanalysis data is accessed, the next step is to extract the runoff grids lying within Canada. In order to do this, a data-frame “grids.cama.input” is prepared with coordinate extent of Canada. The R code is provided in **Figure 4.5**.

```
grids.cama.input=data.frame(lon=rep(seq(-180,179.75,by=1),times=180,lat=rep(seq(90,-89,by=-1),each=360))
```

Figure 4.5: R code for extracting runoff grids lying within Canada

4.4 Converting input runoff from numeric to binary format

After extracting the runoff values, the next step is to convert the numeric data to binary format, in order to be used as input to the flood model. The R-code presented in **Figure 4.6** converts the numeric runoff data to binary using the function “writeBIN”.

```
SUB.write.daily.bin=function(runoff.day,date.day,scenario)
writeBin(object=runoff.day, endian="little", size=4, con=paste("C:/Reanalysis/NARR /CamaFlood
runoff ",100YR,"/Roff___",date.day,".one",sep=""))
```

Figure 4.6: R code for converting input runoff from numeric to binary format

4.5 Model simulations

Once the inputs are prepared, the data input, location and outputs should be specified in the WinSCP, so that they can be accessed by the CaMa-Flood model. Desirable outputs if any, can also be fixed by making changes in this file. Modules and paths should be set in Mkinclude file before running the CaMa-Flood for runoff simulations as described in **Figure 3.4**. The Input runoff files should be transferred from the destination folder to the CaMa-Flood package through WinSCP as shown in **Figure 4.7**.

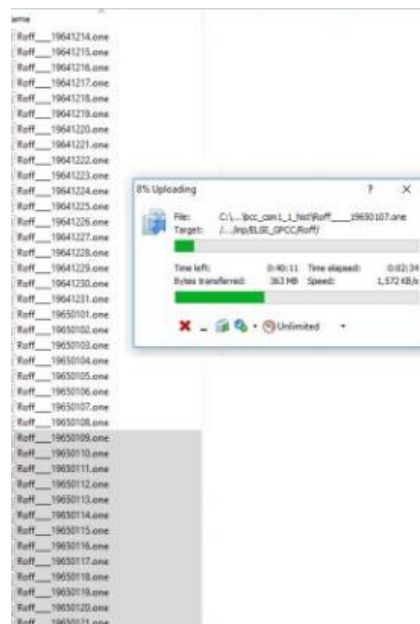


Figure 4.7: Transferring input files to the CaMa-Flood package in input folder

The following steps can be followed for performing a simulation in CaMa-Flood:

- Launch PUTTY as shown in **Figure 3.2**. Enter the login and password details corresponding to the host name. In this case, the host is Graham server of the SHARCNET. In doing so, it will open a screen, where we have to reenter the password to access the server as shown in **Figure 4.8**.
- After logging in to the server, the compilation and creation of CaMa-Flood model is established as highlighted in Yellow colour in **Figure 4.9**. Next, “bash compile.sh yes” is used to start running CaMa-Flood model as shown in **Figure 4.10**. A unique job-id and status also appears on the screen that will show the progress of simulation.

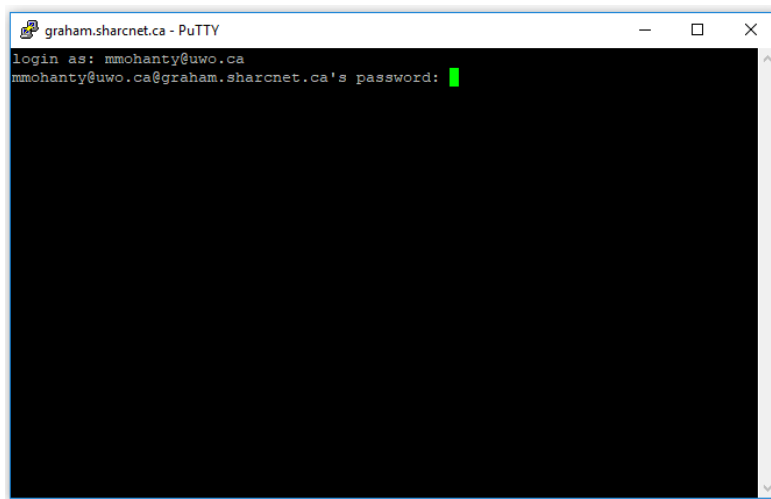


Figure 4.8: Logging into SHARCNET for accessing Graham server

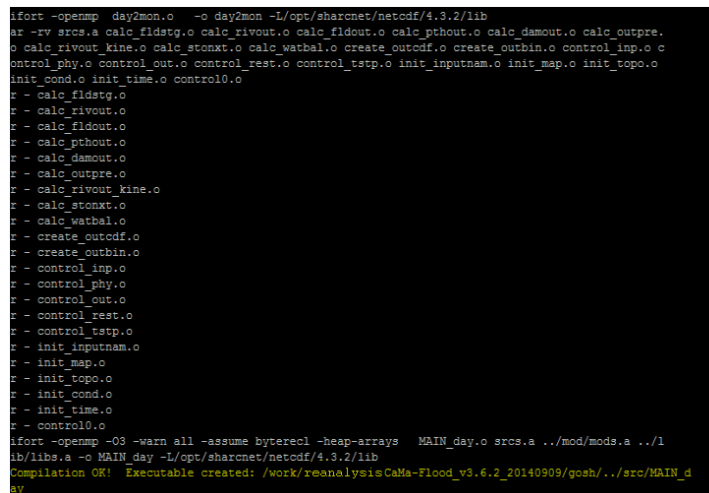


Figure 4.9: Code compilation and creating executables in SHARCNET

```

ifort -openmp -c -O3 -warn all -assume byterecl -heap-arrays -I/opt/sharcnet/netcdf/4.3.2/include
de day2mon.f90 -o day2mon.o
ifort -openmp day2mon.o -o day2mon -L/opt/sharcnet/netcdf/4.3.2/lib
ar -rv srcs.a calc_fldstg.o calc_rivout.o calc_fldout.o calc_pthout.o calc_damout.o calc_outpre.
o calc_rivout_kine.o calc_stonxt.o calc_watbal.o create_outcdf.o create_outbin.o control_inp.o c
control_phy.o control_out.o control_rest.o control_tstp.o init_inputnam.o init_map.o init_topo.o
init_cond.o init_time.o control0.o
E - calc_fldstg.o
E - calc_rivout.o
E - calc_fldout.o
E - calc_pthout.o
E - calc_damout.o
E - calc_outpre.o
E - calc_rivout_kine.o
E - calc_stonxt.o
E - calc_watbal.o
E - create_outcdf.o
E - create_outbin.o
E - control_inp.o
E - control_phy.o
E - control_out.o
E - control_rest.o
E - control_tstp.o
E - init_inputnam.o
E - init_map.o
E - init_topo.o
E - init_cond.o
E - init_time.o
E - control0.o
ifort -openmp -O3 -warn all -assume byterecl -heap-arrays MAIN_day.o srcs.a ../mod/mods.a ../l
ib/libs.a -o MAIN_day -L/opt/sharcnet/netcdf/4.3.2/lib
Compilation OK! Executable created: /work/reanalysis/CaMa-Flood_v3.6.2_20140909/gosh/.../src/MAI
ay
-bash-4.1$ sqsub -q threaded -n 24 -r 4h --mpp=16g -o output.txt bash global_15min.sh
submitted as jobid 337887
-bash-4.1$ sqjobs
jobid queue state ncpus nodes time command
-----
337887 threaded R 24 cop28 17s bash global_15min.sh
-bash-4.1$

```

Figure 4.10: Final code for running CaMa-Flood model simulation in PuTTY software

- Once the model simulations are complete, we can go back to the folder meant to store the relevant outputs (**Figure 4.11**). The results are in the binary format, which can be converted to numeric format and GeoTIFF as per the code in **Figure 4.12**.

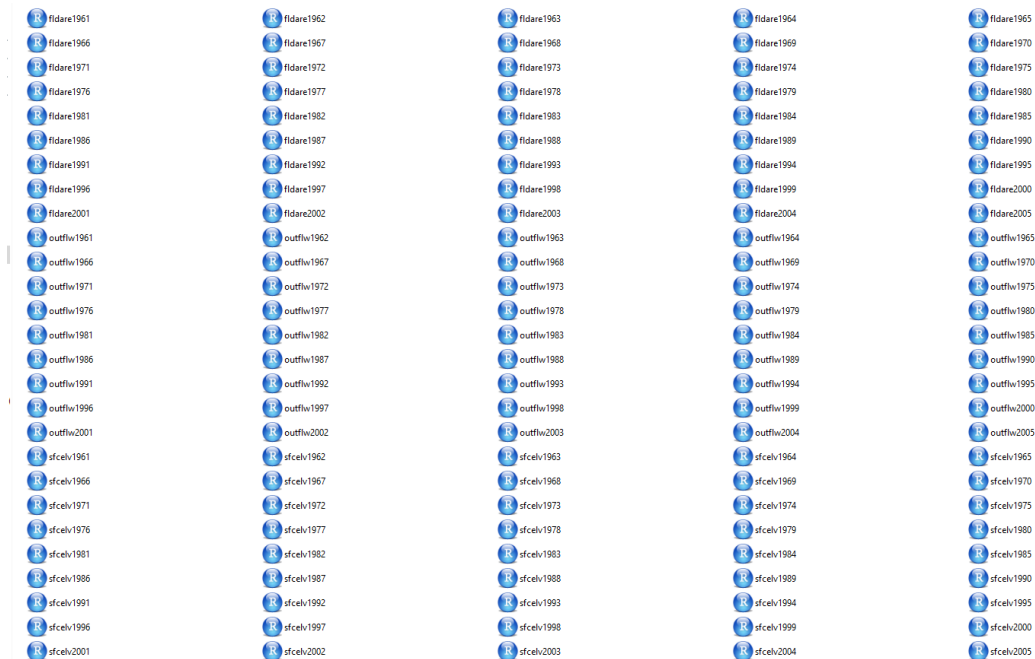


Figure 4.11: Flood simulation outputs

```

function [temp,header]=ctltoRaster(Df,Latlim,Lonlim,xx,yy,outfile)
%file_name='C:\Runoff\NARR_100YR_result\flddph.ctl';
tempS=Df(:, :, 1, :);
temp=mean(tempS,4);
[m,n]=size(temp);
mValue=max(max(temp));
for i=1:m
    for j=1:n
        if abs(temp(i,j)-mValue)<0.001
            temp(i,j)=0;
        end
    end
end
end
%[x,y] = meshgrid([72:0.005:135.9950],[-179.875:0.25:179.8750]);

% surf(x,y, temp)
%
% [Plg,Plt]=meshgrid([-89.875:0.25:89.875],[-179.875:0.25:179.8750]);
%
% m_proj('hammer-aitoff','clongitude',-150);
% m_pcolor(Plg,Plt,temp);shading flat;
% hold on;
% m_coast('patch',[.6 1 .6]);
% m_grid('xaxis','middle');
%
% % add a standard colorbar.
% h=colorbar('h');
% set(get(h,'title'),'string','NARR_2010');
%
% hold off

R = georasterref('RasterSize', [xx yy ], ...
    'RasterInterpretation', 'cells', ...
    'Latlim',Latlim,'Lonlim',Lonlim, ...
    'ColumnsStartFrom', 'north');
geotiffwrite(outfile,temp',R)

```

Figure 4.12: R code for converting binary data to GeoTIFF format

- The GeoTIFF file can be opened in Arc GIS to visualize the values and perform impact analysis. Since the result does not come with any geographic projection, it is necessary to define a new projection 'D_WGS_1984' to ensure the boundary of Canada and floodplain maps match accurately. A larger domain of reanalysis data extent is considered, hence the results within Canada can be clipped by using 'Clip Raster' option. The final floodplain map for 2010 year is shown in **Figure 4.13**.

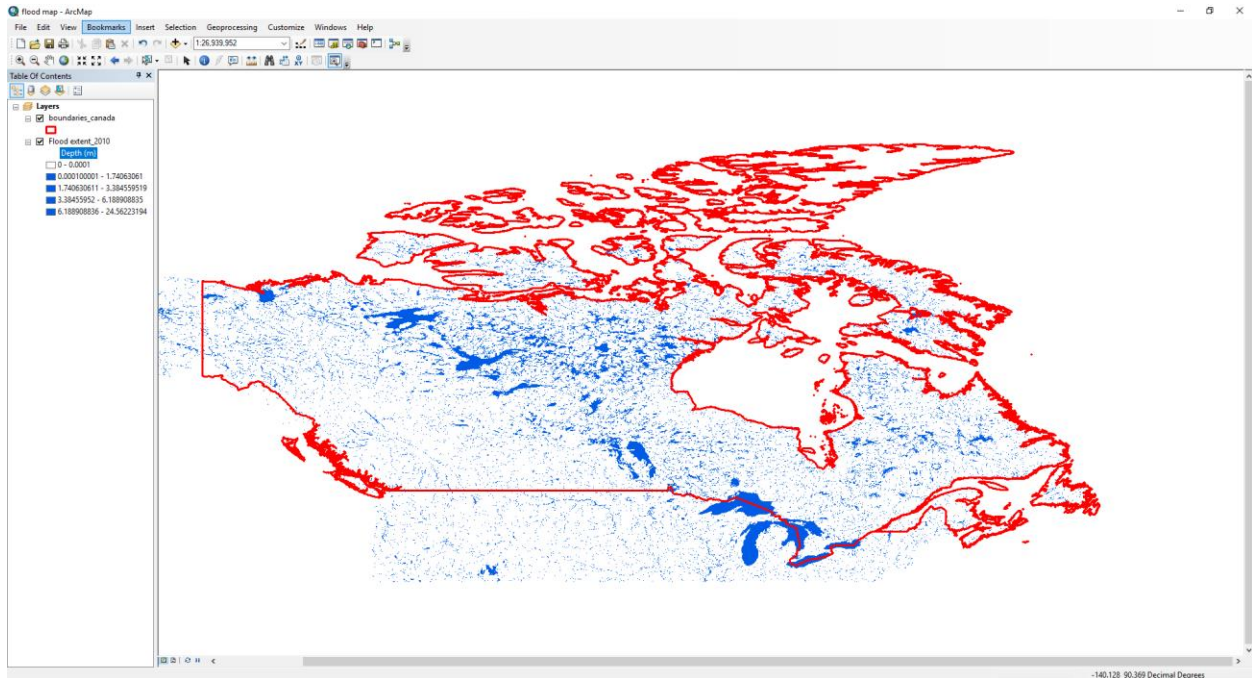


Figure 4.13: Floodplain map of 2010 for Canada by using NARR reanalysis runoff

Chapter 5 Closing remarks

With the global rise of flood-prone regions, it has now become more important than before to perform the floodplain mapping at large scales. This process has become much easier with the public release of datasets, and availability of sophisticated global flood models. In this report, we provide a detailed overview of the past and ongoing research on large-scale floodplain mapping, and availability of public datasets to serve as model inputs. In doing so, we also present a sample simulation of the CaMa-Flood model by utilising freely available NARR reanalysis product data. The CaMa-Flood model explicitly parameterizes the sub-grid scale topography of a floodplain, thus describing floodplain inundation dynamics. The relationship between water storage, water level, and flooded area in the model is decided on the basis of the sub-grid scale topographic parameters based on 1 km resolution digital elevation model. In this report, we use R programming language to read, prepare inputs, and analyse most of the data. The major advantage of R is that it resides in public domain; it also allows easy integration with other languages like, C/C++, Java, Python, and enables communication with many data sources and other statistical packages. In the last part, we also present a new methodology to convert the output data into a simple GeoTIFF format, which can be used by any non-computational expert. This report may be considered by any water professional, working on floodplain mapping researches, for delineating precise flood-maps and quantifying impact assessments such as population and economic damages.

Chapter 6 References

- Aerts, J. C., Botzen, W. W., Emanuel, K., Lin, N., De Moel, H., & Michel-Kerjan, E. O. (2014). Evaluating flood resilience strategies for coastal megacities. *Science*, 344(6183), 473-475.
- Alfieri, L., Bisselink, B., Dottori, F., Naumann, G., de Roo, A., Salamon, P., ... & Feyen, L. (2017). Global projections of river flood risk in a warmer world. *Earth's Future*, 5(2), 171-182.
- Alfieri, L., Burek, P., Feyen, L., & Forzieri, G. (2015). Global warming increases the frequency of river floods in Europe. *Hydrology & Earth System Sciences Discussions*, 12(1).
- Alfieri, L., Dottori, F., Betts, R., Salamon, P., & Feyen, L. (2018). Multi-model projections of river flood risk in Europe under global warming. *Climate*, 6(1), 6.
- Alfieri, L., Feyen, L., Dottori, F., & Bianchi, A. (2015). Ensemble flood risk assessment in Europe under high end climate scenarios. *Global Environmental Change*, 35, 199-212.
- Alfieri, L., Salamon, P., Bianchi, A., Neal, J., Bates, P., & Feyen, L. (2014). Advances in pan-European flood hazard mapping. *Hydrological processes*, 28(13), 4067-4077.
- Andreadis, K. M., Schumann, G. J. P., Stampoulis, D., Bates, P. D., Brakenridge, G. R., & Kettner, A. J. (2017). Can atmospheric reanalysis data sets be used to reproduce flooding over large scales?. *Geophysical Research Letters*, 44(20), 10-369.
- Apel, H., Aronica, G.T., Kreibich, H., & Thielen, A.H. (2009). Flood risk analyses-How detailed do we need to be? *Natural Hazards*, 49, 79-98.
- Arnell, N. W., & Lloyd-Hughes, B. (2014). The global-scale impacts of climate change on water resources and flooding under new climate and socio-economic scenarios. *Climatic Change*, 122(1-2), 127-140.
- Bates, P. D., Horritt, M. S., & Fewtrell, T. J. (2010). A simple inertial formulation of the shallow water equations for efficient two-dimensional flood inundation modelling. *Journal of Hydrology*, 387(1-2), 33-45.
- Bazgeer, S., Oskuee, E. A., Hagigat, M., & Darban Astane, A. R. (2012). Assessing the performance of spatial interpolation methods for mapping precipitation data: a case study in Fars Province, Iran. *Trends in Applied Sciences Research*, 7(6), 467-475.
- Bengtsson, L., Hagemann, S., & Hodges, K. I. (2004). Can climate trends be calculated from reanalysis data?. *Journal of Geophysical Research: Atmospheres*, 109(D11).
- Bouwer, L. M., Bubeck, P., & Aerts, J. C. (2010). Changes in future flood risk due to climate and development in a Dutch polder area. *Global Environmental Change*, 20(3), 463-471.
- Brown, S., Nicholls, R. J., Hanson, S., Brundrit, G., Dearing, J. A., Dickson, M. E., ... & Jiménez, J. A. (2014). Shifting perspectives on coastal impacts and adaptation. *Nature Climate Change*, 4(9), 752
- Buckland, J., & Rahman, M. (1999). Community-based disaster management during the 1997 Red River Flood in Canada. *Disasters*, 23(2), 174-191.

- Burn, D. H., & Whitfield, P. H. (2016). Changes in floods and flood regimes in Canada. *Canadian Water Resources Journal/Revue canadienne des ressources hydriques*, 41(1-2), 139-150.
- Cohen, S., Willgoose, G., & Hancock, G. (2013). Soil–landscape response to mid and late Quaternary climate fluctuations based on numerical simulations. *Quaternary research*, 79(3), 452-457.
- Compo, G. P., Whitaker, J. S., Sardeshmukh, P. D., Matsui, N., Allan, R. J., Yin, X., ... & Brönnimann, S. (2011). The twentieth century reanalysis project. *Quarterly Journal of the Royal Meteorological Society*, 137(654), 1-28.
- Cunderlik, J. M., & Simonovic, S. P. (2007). Inverse flood risk modelling under changing climatic conditions. *Hydrological Processes: An International Journal*, 21(5), 563-577.
- Dee, D. P., Uppala, S. M., Simmons, A. J., Berrisford, P., Poli, P., Kobayashi, S., ... & Bechtold, P. (2011). The ERA-Interim reanalysis: Configuration and performance of the data assimilation system. *Quarterly Journal of the royal meteorological society*, 137(656), 553-597.
- DHI (2003). 1D-2D Modelling. User Manual. DHI Water & Environment, Horsholm, Denmark.
- Dottori, F., Salamon, P., Bianchi, A., Alfieri, L., Hirpa, F. A., & Feyen, L. (2016). Development and evaluation of a framework for global flood hazard mapping. *Advances in water resources*, 94, 87-102.
- Eisner, S., Voss, F., & Kynast, E. (2012). Statistical bias correction of global climate projections—consequences for large scale modeling of flood flows. *Advances in Geosciences*, 31, 75-82.
- Emerton, R., Cloke, H. L., Stephens, E. M., Zsoter, E., Woolnough, S. J., & Pappenberger, F. (2017). Complex picture for likelihood of ENSO-driven flood hazard. *Nature communications*, 8(1), 1-9.
- Essou, G. R., Sabarly, F., Lucas-Picher, P., Brissette, F., & Poulin, A. (2016). Can precipitation and temperature from meteorological reanalyses be used for hydrological modeling?. *Journal of Hydrometeorology*, 17(7), 1929-1950.
- Feyen, L., Dankers, R., Bódis, K., Salamon, P., & Barredo, J. I. (2012). Fluvial flood risk in Europe in present and future climates. *Climatic change*, 112(1), 47-62.
- Gaur, A., Gaur, A., & Simonovic, S. P. (2018). Future Changes in Flood Hazards across Canada under a Changing Climate. *Water*, 10(10), 1441.
- Gaur, A., Gaur, A., Yamazaki, D., & Simonovic, S. P. (2019). Flooding Related Consequences of Climate Change on Canadian Cities and Flow Regulation Infrastructure. *Water*, 11(1), 63.
- Gichamo, T. Z., Popescu, I., Jonoski, A., & Solomatine, D. (2012). River cross-section extraction from the ASTER global DEM for flood modeling. *Environmental Modelling & Software*, 31, 37-46
- Haer, T., Botzen, W. W., Van Roomen, V., Connor, H., Zavala-Hidalgo, J., Eilander, D. M., & Ward, P. J. (2018). Coastal and river flood risk analyses for guiding economically optimal

flood adaptation policies: a country-scale study for Mexico. *Philosophical Transactions of the Royal Society A: Mathematical, Physical and Engineering Sciences*, 376(2121), 20170329.

Haer, T., Botzen, W. W., Zavala-Hidalgo, J., Cusell, C., & Ward, P. J. (2017). Economic evaluation of climate risk adaptation strategies: Cost-benefit analysis of flood protection in Tabasco, Mexico. *Atmósfera*, 30(2), 101-120.

Haznet (2019) < <http://haznet.ca/flood-mapping-canada-qa/>> last accessed on 23 November 2019

Hirabayashi, Y., Mahendran, R., Koirala, S., Konoshima, L., Yamazaki, D., Watanabe, S., ... & Kanae, S. (2013). Global flood risk under climate change. *Nature Climate Change*, 3(9), 816-821.

Hirpa, F. A., Salamon, P., Alfieri, L., Pozo, J. T. D., Zsoter, E., & Pappenberger, F. (2016). The effect of reference climatology on global flood forecasting. *Journal of Hydrometeorology*, 17(4), 1131-1145.

Ho, L. T., & Umitsu, M. (2011). Micro-landform classification and flood hazard assessment of the Thu Bon alluvial plain, central Vietnam via an integrated method utilizing remotely sensed data. *Applied Geography*, 31(3), 1082-1093.

Hoch, J. M., & Trigg, M. A. (2019). Advancing global flood hazard simulations by improving comparability, benchmarking, and integration of global flood models. *Environmental Research Letters*, 14(3), 034001.

Hodges, K. I., Hoskins, B. J., Boyle, J., & Thorncroft, C. (2003). A comparison of recent reanalysis datasets using objective feature tracking: Storm tracks and tropical easterly waves. *Monthly Weather Review*, 131(9), 2012-2037.

Hunter, J. R., Woodworth, P. L., Wahl, T., & Nicholls, R. J. (2017). Using global tide gauge data to validate and improve the representation of extreme sea levels in flood impact studies. *Global and Planetary Change*, 156, 34-45.

Hunter, N. M., Horritt, M. S., Bates, P. D., Wilson, M. D., & Werner, M. G. (2005). An adaptive time step solution for raster-based storage cell modelling of floodplain inundation. *Advances in water resources*, 28(9), 975-991.

Jongman, B., Ward, P. J., & Aerts, J. C. (2012). Global exposure to river and coastal flooding: Long term trends and changes. *Global Environmental Change*, 22(4), 823-835.

Jongman, B., Winsemius, H. C., Aerts, J. C., De Perez, E. C., Van Aalst, M. K., Kron, W., & Ward, P. J. (2015). Declining vulnerability to river floods and the global benefits of adaptation. *Proceedings of the National Academy of Sciences*, 112(18), E2271-E2280.

Jung, H. C., Alsdorf, D., Moritz, M., Lee, H., & Vassolo, S. (2011). Analysis of the relationship between flooding area and water height in the Logone floodplain. *Physics and Chemistry of the Earth, Parts A/B/C*, 36(7-8), 232-240.

Karlsson, J.M., Arnberg, W., 2011. Quality analysis of SRTM and HYDRO1K : a case study of flood inundation in Mozambique. *International Journal of Remote Sensing*, 32, 267–285.

- Kim, Y., & Chung, E. S. (2014). An index-based robust decision making framework for watershed management in a changing climate. *Science of the total environment*, 473, 88-102
- Kinoshita, Y., Tanoue, M., Watanabe, S., & Hirabayashi, Y. (2018). Quantifying the effect of autonomous adaptation to global river flood projections: application to future flood risk assessments. *Environmental Research Letters*, 13(1), 014006
- Koirala, S., Hirabayashi, Y., Mahendran, R., & Kanae, S. (2014). Global assessment of agreement among streamflow projections using CMIP5 model outputs. *Environmental Research Letters*, 9(6), 064017.
- Lehner, B., Verdin, K., & Jarvis, A. (2006). *HydroSHEDS technical documentation*, version 1.0. World Wildlife Fund US, Washington, DC, 1-27.
- Lim, W. H., Yamazaki, D., Koirala, S., Hirabayashi, Y., Kanae, S., Dadson, S. J., ... & Sun, F. (2018). Long-term changes in global socioeconomic benefits of flood defenses and residual risk based on CMIP5 climate models. *Earth's Future*, 6(7), 938-954.
- Manitoba Infrastructure and Transportation. (2013). *Manitoba 2011 Flood Review Task Force Report*.
- Masutomi, Y., Inui, Y., Takahashi, K., & Matsuoka, Y. (2007). *Global Drainage Basin Database (GDBD)*.
- Milly, P. C. D., Wetherald, R. T., Dunne, K. A., & Delworth, T. L. (2002). Increasing risk of great floods in a changing climate. *Nature*, 415(6871), 514-517.
- Mohanty, M. P., Vittal, H., Yadav, V., Ghosh, S., Rao, G. S., & Karmakar, S. (2020). A new bivariate risk classifier for flood management considering hazard and socio-economic dimensions. *Journal of Environmental Management*, 255, 109733.
- Mokrech, M., Kebede, A. S., Nicholls, R. J., Wimmer, F., & Feyen, L. (2015). An integrated approach for assessing flood impacts due to future climate and socio-economic conditions and the scope of adaptation in Europe. *Climatic Change*, 128(3-4), 245-260.
- Muis, S., Güneralp, B., Jongman, B., Aerts, J. C., & Ward, P. J. (2015). Flood risk and adaptation strategies under climate change and urban expansion: A probabilistic analysis using global data. *Science of the Total Environment*, 538, 445-457
- Munich Re (2018). *NatCatSERVICE database*. Munich RE, Munich
- Nkiaka, E., Nawaz, N. R., & Lovett, J. C. (2017). Evaluating global reanalysis datasets as input for hydrological modelling in the Sudano-Sahel region. *Hydrology*, 4(1), 13.
- NRCan (2018) *Natural Resources Canada Federal Floodplain mapping Framework* <http://ftp.geogratis.gc.ca/pub/nrcan_rncan/publications/ess_sst/308/308128/gip_112_v2_0_en.pdf> accessed on 10 May 2020.
- Ntajal, J., Lamptey, B. L., Mahamadou, I. B., & Nyarko, B. K. (2017). Flood disaster risk mapping in the Lower Mono River Basin in Togo, West Africa. *International Journal of Disaster Risk Reduction*, 23, 93-103.
- Paiva, R. C., Collischonn, W., & Tucci, C. E. (2011). Large scale hydrologic and hydrodynamic modeling using limited data and a GIS based approach. *Journal of Hydrology*, 406(3-4), 170-181.

- Paiva, R.C.D., Collischonn, W., Tucci, C.E.M., 2011. Large scale hydrologic and hydrodynamic modeling using limited data and a GIS based approach. *J. Hydrol.* 406, 170–181. doi:10.1016/j.jhydrol.2011.06.007
- Pappenberger, F., Dutra, E., Wetterhall, F., & Cloke, H. L. (2012). Deriving global flood hazard maps of fluvial floods through a physical model cascade. *Hydrology and Earth System Sciences*, 16(11), 4143-4156.
- Patro, S., Chatterjee, C., Singh, R., & Raghuwanshi, N. S. (2009). Hydrodynamic modelling of a large flood-prone river system in India with limited data. *Hydrological Processes: An International Journal*, 23(19), 2774-2791.
- Pomeroy, J. W., Stewart, R. E., & Whitfield, P. H. (2016). The 2013 flood event in the South Saskatchewan and Elk River basins: Causes, assessment and damages. *Canadian Water Resources Journal/Revue canadienne des ressources hydriques*, 41(1-2), 105-117.
- Public Safety Canada (2017) Floods <<https://www.publicsafety.gc.ca/cnt/mrgnc-mngmnt/ntrl-hzrds/fld-en.aspx>> accessed on 10 December 2019
- Public Safety Canada (2019) Federal Floodplain mapping Guidelines Series <<https://www.publicsafety.gc.ca/cnt/mrgnc-mngmnt/dsstr-prvntn-mtgn/ndmp/fldpln-mppng-en.aspx>> accessed on 7 June 2020.
- Rienecker, M. M., Suarez, M. J., Todling, R., Bacmeister, J., Takacs, L., Liu, H. C., ... & Stajner, I. (2008). The GEOS-5 Data Assimilation System: Documentation of Versions 5.0. 1, 5.1. 0, and 5.2. 0.
- Rojas, R., Feyen, L., & Watkiss, P. (2013). Climate change and river floods in the European Union: Socio-economic consequences and the costs and benefits of adaptation. *Global Environmental Change*, 23(6), 1737-1751.
- Sabarly, F., Essou, G., Lucas-Picher, P., Poulin, A., & Brissette, F. (2016). Use of four reanalysis datasets to assess the terrestrial branch of the water cycle over Quebec, Canada. *Journal of Hydrometeorology*, 17(5), 1447-1466.
- Saha, S., Moorthi, S., Pan, H. L., Wu, X., Wang, J., Nadiga, S., ... & Liu, H. (2010). The NCEP climate forecast system reanalysis. *Bulletin of the American Meteorological Society*, 91(8), 1015-1058.
- Samiran, D., & Simonovic, S. P. (2012). Assessment of uncertainty in flood flows under climate change impacts in the Upper Thames River basin, Canada. *British Journal of Environment and Climate Change*, 2(4), 318-338.
- Sampson, C. C., Smith, A. M., Bates, P. D., Neal, J. C., Alfieri, L., & Freer, J. E. (2015). A high-resolution global flood hazard model. *Water resources research*, 51(9), 7358-7381.
- Shao, W., Xian, S., Lin, N., & Small, M. J. (2017). A sequential model to link contextual risk, perception and public support for flood adaptation policy. *Water research*, 122, 216-22.
- Simonovic, S. P., & Li, L. (2003). Methodology for assessment of climate change impacts on large-scale flood protection system. *Journal of Water Resources Planning and Management*, 129(5), 361-371.

- Skakun, S., Kussul, N., Shelestov, A., & Kussul, O. (2014). Flood hazard and flood risk assessment using a time series of satellite images: A case study in Namibia. *Risk Analysis*, 34(8), 1521-1537.
- Suarez, M. (2008). File specification for MERRA products, version 2.1.
- Tarekegn, T. H., Haile, A. T., Rientjes, T., Reggiani, P., & Alkema, D. (2010). Assessment of an ASTER-generated DEM for 2D hydrodynamic flood modeling. *International Journal of Applied Earth Observation and Geoinformation*, 12(6), 457-465.
- Taylor, K. E., Stouffer, R. J., & Meehl, G. A. (2012). An overview of CMIP5 and the experiment design. *Bulletin of the American Meteorological Society*, 93(4), 485-498.
- Trigg, M. A., Birch, C. E., Neal, J. C., Bates, P. D., Smith, A., Sampson, C. C., ... & Ward, P. J. (2016). The credibility challenge for global fluvial flood risk analysis. *Environmental Research Letters*, 11(9), 094014.
- Ullah, S., Farooq, M., Sarwar, T., Tareen, M. J., & Wahid, M. A. (2016). Flood modeling and simulations using hydrodynamic model and ASTER DEM-A case study of Kalpani River. *Arabian Journal of Geosciences*, 9(6), 439.
- UNISDR – The United Nations Office for Disaster Risk Reduction: The human cost of weather-related disasters 1995–2015, available at: https://www.unisdr.org/files/46796_cop21weatherdisastersreport2015.pdf (last access: 28 June 2019), 2015.
- Uppala, S. M., Kållberg, P. W., Simmons, A. J., Andrae, U., Bechtold, V. D. C., Fiorino, M., ... & Li, X. (2005). The ERA-40 re-analysis. *Quarterly Journal of the Royal Meteorological Society: A journal of the atmospheric sciences, applied meteorology and physical oceanography*, 131(612), 2961-3012.
- US Army Corps of Engineers (2019) HEC-GeoRAS <<https://www.hec.usace.army.mil/software/hec-georas/>> accessed on 8 June 2020.
- Wang, W., Yang, X., Yao, T. (2012). Evaluation of ASTER GDEM and SRTM and their suitability in hydraulic modelling of a glacial lake outburst flood in southeast Tibet. *Hydrological Processes*, 225, 213–225.
- Wang, X. L., Swail, V. R., & Zwiers, F. W. (2006). Climatology and changes of extratropical cyclone activity: Comparison of ERA-40 with NCEP–NCAR reanalysis for 1958–2001. *Journal of Climate*, 19(13), 3145-3166.
- Ward, P. J., de Perez, E. C., Dottori, F., Jongman, B., Luo, T., Safaie, S., & Uhlemann-Elmer, S. (2018). The need for mapping, modeling, and predicting flood hazard and risk at the global scale. *Global flood hazard: Applications in modeling, mapping, and forecasting*, 1-15.
- Ward, P. J., Jongman, B., Aerts, J. C., Bates, P. D., Botzen, W. J., Loaiza, A. D., ... & Winsemius, H. C. (2017). A global framework for future costs and benefits of river-flood protection in urban areas. *Nature climate change*, 7(9), 642-646.
- Ward, P. J., Jongman, B., Weiland, F. S., Bouwman, A., van Beek, R., Bierkens, M. F., ... & Winsemius, H. C. (2013). Assessing flood risk at the global scale: model setup, results, and sensitivity. *Environmental Research Letters*, 8(4), 044019.

- Wdowinski, S., Bray, R., Kirtman, B. P., & Wu, Z. (2016). Increasing flooding hazard in coastal communities due to rising sea level: Case study of Miami Beach, Florida. *Ocean & Coastal Management*, 126, 1-8.
- Willner, S. N., Levermann, A., Zhao, F., & Frieler, K. (2018). Adaptation required to preserve future high-end river flood risk at present levels. *Science advances*, 4(1), eaao1914.
- Wing, O. E., Bates, P. D., Sampson, C. C., Smith, A. M., Johnson, K. A., & Erickson, T. A. (2017). Validation of a 30 m resolution flood hazard model of the conterminous United States. *Water Resources Research*, 53(9), 7968-7986.
- Winsemius, H. C., Aerts, J. C., Van Beek, L. P., Bierkens, M. F., Bouwman, A., Jongman, B., ... & Ward, P. J. (2016). Global drivers of future river flood risk. *Nature Climate Change*, 6(4), 381-385.
- Winsemius, H. C., Van Beek, L. P. H., Jongman, B., Ward, P. J., & Bouwman, A. (2013). A framework for global river flood risk assessments. *Hydrology and Earth System Sciences*, 17(5), 1871-1892.
- Woodhead, S., Asselman, N., Zech, Y., Soares-Frazao, S., Bates, P., & Kortenhaus, A. (2007). Evaluation of inundation models. FLOODsite Project Report T08-07-01.
- Wu, H., Kimball, J. S., Li, H., Huang, M., Leung, L. R., & Adler, R. F. (2012). A new global river network database for macroscale hydrologic modeling. *Water resources research*, 48(9).
- Yamazaki, D., de Almeida, G. A., & Bates, P. D. (2013). Improving computational efficiency in global river models by implementing the local inertial flow equation and a vector-based river network map. *Water Resources Research*, 49(11), 7221-7235.
- Yamazaki, D., Ikeshima, D., Sosa, J., Bates, P. D., Allen, G. H., & Pavelsky, T. M. (2019). MERIT Hydro: a high-resolution global hydrography map based on latest topography dataset. *Water Resources Research*, 55(6), 5053-5073.
- Yamazaki, D., Ikeshima, D., Tawatari, R., Yamaguchi, T., O'Loughlin, F., Neal, J. C., ... & Bates, P. D. (2017). A high-accuracy map of global terrain elevations. *Geophysical Research Letters*, 44(11), 5844-5853.
- Yamazaki, D., Kanae, S., Kim, H., & Oki, T. (2011). A physically based description of floodplain inundation dynamics in a global river routing model. *Water Resources Research*, 47(4).
- Yamazaki, D., Oki, T., & Kanae, S. (2009). Deriving a global river network map and its sub-grid topographic characteristics from a fine-resolution flow direction map. *Hydrology and Earth System Sciences*, 13(11), 2241.
- Yamazaki, D., O'Loughlin, F., Trigg, M. A., Miller, Z. F., Pavelsky, T. M., & Bates, P. D. (2014). Development of the global width database for large rivers. *Water Resources Research*, 50(4), 3467-3480.
- Yan, K., Baldassarre, G. Di, Solomatine, D.P. (2013). Exploring the potential of SRTM topographic data for flood inundation modelling under uncertainty 849–862. doi:10.2166/hydro.2013.137
- Youssef, A. M., Pradhan, B., & Hassan, A. M. (2011). Flash flood risk estimation along the St.

Katherine road, southern Sinai, Egypt using GIS based morphometry and satellite imagery. *Environmental Earth Sciences*, 62(3), 611-623.

Zsótér, E., Pappenberger, F., Smith, P., Emerton, R. E., Dutra, E., Wetterhall, F., ... & Balsamo, G. (2016). Building a multimodel flood prediction system with the TIGGE archive. *Journal of Hydrometeorology*, 17(11), 2923-2940.

Appendix A: List of freely available global data in floodplain mapping

Table A1. List of freely available global data in floodplain mapping

Data	Specific data	Name	Source
Meteorological	Rainfall	Tropical Rainfall Measuring Mission (TRMM)	https://climatedataguide.ucar.edu/climate-data/trmm-tropical-rainfall-measuring-mission
		Climatic Research Unit Time-series (CRU)	https://climatedataguide.ucar.edu/climate-data/cru-ts-gridded-precipitation-and-other-meteorological-variables-1901
		Global Historical Climatology Network (GHCN-M)	https://www.ncdc.noaa.gov/data-access/land-based-station-data/land-based-datasets/global-historical-climatology-network-ghcn
		Global Precipitation Climatology Centre (GPCC)	https://climatedataguide.ucar.edu/climate-data/gpcc-global-precipitation-climatology-centre
		University of Delaware Precipitation (UDEL)	https://psl.noaa.gov/data/gridded/data.UDel_AirT_Precip.html
		CPC Global Unified gauge-based precipitation (CPC-Global)	https://psl.noaa.gov/data/gridded/data.cpc.globalprecip.html
		Global Precipitation Measurement (GPM)	https://gpm.nasa.gov/data-access/downloads/gpm

Hydrological	Run-off	ERA-Interim	http://apps.ecmwf.int/datasets/
		CFSR	http://cfs.ncep.noaa.gov/cfsr/
		MERRA	http://disc.sci.gsfc.nasa.gov/mdisc/overview/index.shtml
		NARR	ftp.cdc.noaa.gov/NARR
		Twentieth Century Reanalysis Version v2c (20CRV2)	https://climatedataguide.ucar.edu/climate-data/noaa-20th-century-reanalysis-version-2-and-2c
		EU-WATCH	http://www.eu-watch.org/data_availability
		JRA-25	https://rda.ucar.edu/datasets/ds625.0/
		GloFAS	https://www.globalfloods.eu/
	Snow-melt	Snow Data Assimilation System (SNODAS)	https://nsidc.org/data/G02158
		Japanese Global Snow Cover Extent for Climate Dataset (GHRM5C)	https://nsidc.org/data/G02158 http://kuroshio.eorc.jaxa.jp/JASMES/index.html
		NOAA AMSR2 Snow Products	https://www.ospo.noaa.gov/Products/atmosphere/gpds/
		Global 4KM Multisensor Automated Snow/Ice Map Product (GMASI)	http://satepsanone.nesdis.noaa.gov/
		MODIS Snow Products Collection 6	https://nsidc.org/data/modis/data_summaries
		GRACE	http://podaac.jpl.nasa.gov/grace
	Tide elevation	Global sea level record	https://climatedataguide.ucar.edu/climate-data/tide-gauge-sea-level-data
		Global Extreme Sea Level Analysis (GESLA)	https://gesla.org/

Topographic	Digital elevation models	Shuttle Radar Topography Mission elevation Data (90m)	http://srtm.csi.cgiar.org/
		Shuttle Radar Topography Mission elevation Data (30m)	https://www2.jpl.nasa.gov/srtm/
		Multi-Error-Removed Improved-Terrain DEM	http://hydro.iis.u-tokyo.ac.jp/~yamadai/MERIT_DEM/
		Advanced Spaceborne Thermal Emission and Reflection Radiometer (ASTER)	https://asterweb.jpl.nasa.gov/gdem.asp
		ALOS Global Digital Surface Model	https://www.eorc.jaxa.jp/ALOS/en/aw3d30/index.htm
Demographic	Population	Worldpop	https://www.worldpop.org/geodata/listing?id=29
		Gridded Population of the World (GPW)	https://sedac.ciesin.columbia.edu/data/set/gpw-v4-population-count-rev11
		UNEP Environmental Data Explorer	http://geodata.grid.unep.ch/results.php
		LandScan	https://landscan.ornl.gov/
		Global human settlement	https://ghsl.jrc.ec.europa.eu/download.php?ds=pop

Appendix B: List of widely used reanalysis datasets

B 1. ERA-Interim reanalysis

ERA-Interim is the latest global reanalysis produced by the European Centre for Medium-Range Weather Forecasts (ECMWF) (Dee et al. 2011). It covers the period from 1979 to the present and is produced by the December 2006 integrated forecast model of ECMWF [Integrated Forecast System (IFS) cy31r2]. ERA-Interim uses a four-dimensional variational data assimilation (4DVAR) approach. The observations assimilated before 2002 come mainly from the data used for ERA-40 (Uppala et al. 2005). ERA-Interim is updated in near-real time, using data from the operational ECMWF forecast system (Dee et al. 2011). The horizontal resolution of ERA-Interim is $0.75^\circ \times 0.75^\circ$ and the data is available for free online at <http://apps.ecmwf.int/datasets/>.

B 2. Climate Forecast System Reanalysis (CFSR) reanalysis

The global CFSR is produced by National Centers for Environmental Prediction (NCEP) from a coupled climate system atmosphere-ocean-land surface model with an interactive sea ice component. It covers the period from 1979 to 2010 and uses a three-dimensional variational data assimilation approach (Saha et al. 2010). Estimates of greenhouse gas concentration changes, aerosols, and solar variations are used as forcings in CFSR. The horizontal resolution of CFSR is 0.313° (longitude) \times 0.312° (latitude), and the CFSR dataset is available for free online at <http://cfs.ncep.noaa.gov/cfsr/>.

B 3. Modern-Era Retrospective analysis for Research and Applications (MERRA) reanalysis

The global MERRA is developed by the Global Modeling and Assimilation Office (GMAO) of the National Aeronautics and Space Administration (NASA) in the US. It allows the use of the GMAO satellite observations in a climate context and improvement in the representation of the hydrological cycle from the first generation of reanalyses (Rienecker et al. 2011). MERRA covers the satellite era (from 1979 to present) and is generated from the Goddard Earth Observing System Model, version 5.2.0 (GEOS-5.2.0), and a data assimilation system based on a three-dimensional variational approach (3DVAR). The Data Assimilation System (DAS); the input data flux; and their sources, observations, and error statistics are well documented in Suarez et al. (2008). The

horizontal resolution of MERRA is $2/3^\circ$ (longitude) \times $1/2^\circ$ (latitude). The datasets are available for free online at <http://disc.sci.gsfc.nasa.gov/mdisc/overview/index.shtml>.

B 4. North American Regional Reanalysis (NARR)

The NARR is a product of NCEP, developed to produce high-resolution data for North America. NARR was developed from major improvements of the global NCEP–NCAR reanalyses (Kalnay et al. 1996; Kistler et al. 2001), both in terms of resolution and precision. In light of these improvements, NARR adequately represents extreme events such as droughts and floods. NARR covers the period from 1979 to the present. The NARR system uses the Eta 32-km atmospheric model with 45 vertical layers and a three-dimensional variational data assimilation approach (Mesinger et al. 2006). That model uses the convection scheme of Betts–Miller–Janjić (BMJ) (Betts and Miller 1986; Janjić 1994). The horizontal resolution of NARR is $32\text{ km} \times 32\text{ km}$. The datasets are available for free online at <ftp.cdc.noaa.gov/NARR>.

Appendix C: Previous Reports in the Series

Samiran Das and Slobodan P. Simonovic (2012). Assessment of Uncertainty in Flood Flows under Climate Change. Water Resources Research Report no. 079, Facility for Intelligent Decision Support, Department of Civil and Environmental Engineering, London, Ontario, Canada, 67 pages. ISBN: (print) 978-0-7714-2960-6; (online) 978-0-7714-2961-3. Rubaiya

Sarwar, Sarah E. Irwin, Leanna King and Slobodan P. Simonovic (2012). Assessment of Climatic Vulnerability in the Upper Thames River basin: Downscaling with SDSM. Water Resources Research Report no. 080, Facility for Intelligent Decision Support, Department of Civil and Environmental Engineering, London, Ontario, Canada, 65 pages. ISBN: (print) 978-0-7714-2962-0; (online) 978-0-7714-2963-7.

Sarah E. Irwin, Rubaiya Sarwar, Leanna King and Slobodan P. Simonovic (2012). Assessment of Climatic Vulnerability in the Upper Thames River basin: Downscaling with LARS-WG. Water Resources Research Report no. 081, Facility for Intelligent Decision Support, Department of Civil and Environmental Engineering, London, Ontario, Canada, 80 pages. ISBN: (print) 978-0-7714-2964-4; (online) 978-0-7714-2965-1.

Samiran Das and Slobodan P. Simonovic (2012). Guidelines for Flood Frequency Estimation under Climate Change. Water Resources Research Report no. 082, Facility for Intelligent Decision Support, Department of Civil and Environmental Engineering, London, Ontario, Canada, 44 pages. ISBN: (print) 978-0-7714-2973-6; (online) 978-0-7714-2974-3.

Angela Peck and Slobodan P. Simonovic (2013). Coastal Cities at Risk (CCaR): Generic System Dynamics Simulation Models for Use with City Resilience Simulator. Water Resources Research Report no. 083, Facility for Intelligent Decision Support, Department of Civil and Environmental Engineering, London, Ontario, Canada, 55 pages. ISBN: (print) 978-0-7714-3024-4; (online) 978-0-7714-3025-1.

Roshan Srivastav and Slobodan P. Simonovic (2014). Generic Framework for Computation of Spatial Dynamic Resilience. Water Resources Research Report no. 085, Facility for Intelligent Decision Support, Department of Civil and Environmental Engineering, London, Ontario, Canada, 81 pages. ISBN: (print) 978-0-7714-3067-1; (online) 978-0-7714-3068-8.

Angela Peck and Slobodan P. Simonovic (2014). Coupling System Dynamics with Geographic Information Systems: CCaR Project Report. Water Resources Research Report no. 086, Facility 56 for Intelligent Decision Support, Department of Civil and Environmental Engineering, London, Ontario, Canada, 60 pages. ISBN: (print) 978-0-7714-3069-5; (online) 978-0-7714-3070-1.

Sarah Irwin, Roshan Srivastav and Slobodan P. Simonovic (2014). Instruction for Watershed Delineation in an ArcGIS Environment for Regionalization Studies. Water Resources Research Report no. 087, Facility for Intelligent Decision Support, Department of Civil and Environmental Engineering, London, Ontario, Canada, 45 pages. ISBN: (print) 978-0-7714-3071-8; (online) 978-0-7714-3072-5.

Andre Schardong, Roshan K. Srivastav and Slobodan P. Simonovic (2014). Computerized Tool for the Development of Intensity-Duration-Frequency Curves under a Changing Climate: Users Manual v.1. Water Resources Research Report no. 088, Facility for Intelligent Decision Support, Department of Civil and Environmental Engineering, London, Ontario, Canada, 68 pages. ISBN: (print) 978-0-7714-3085-5; (online) 978-0-7714-3086-2.

Roshan K. Srivastav, Andre Schardong and Slobodan P. Simonovic (2014). Computerized Tool for the Development of Intensity-Duration-Frequency Curves under a Changing Climate: Technical Manual v.1. Water Resources Research Report no. 089, Facility for Intelligent Decision Support, Department of Civil

and Environmental Engineering, London, Ontario, Canada, 62 pages. ISBN: (print) 978-0-7714-3087-9; (online) 978-0-7714-3088-6.

Roshan K. Srivastav and Slobodan P. Simonovic (2014). Simulation of Dynamic Resilience: A Railway Case Study. Water Resources Research Report no. 090, Facility for Intelligent Decision Support, Department of Civil and Environmental Engineering, London, Ontario, Canada, 91 pages. ISBN: (print) 978-0-7714-3089-3; (online) 978-0-7714-3090-9.

Nick Agam and Slobodan P. Simonovic (2015). Development of Inundation Maps for the Vancouver Coastline Incorporating the Effects of Sea Level Rise and Extreme Events. Water Resources Research Report no. 091, Facility for Intelligent Decision Support, Department of Civil and Environmental Engineering, London, Ontario, Canada, 107 pages. ISBN: (print) 978-0-7714-3092-3; (online) 978-0-7714-3094-7.

Sarah Irwin, Roshan K. Srivastav and Slobodan P. Simonovic (2015). Instructions for Operating the Proposed Regionalization Tool "Cluster-FCM" Using Fuzzy C-Means Clustering and LMoment Statistics. Water Resources Research Report no. 092, Facility for Intelligent Decision Support, Department of Civil and Environmental Engineering, London, Ontario, Canada, 54 pages. ISBN: (print) 978-0-7714-3101-2; (online) 978-0-7714-3102-9. 57

Bogdan Pavlovic and Slobodan P. Simonovic (2016). Automated Control Flow Generation Procedure: Cheakamus Dam Case Study. Water Resources Research Report no. 093, Facility for Intelligent Decision Support, Department of Civil and Environmental Engineering, London, Ontario, Canada, 78 pages. ISBN: (print) 978-0-7714-3113-5; (online) 978-0-7714-3114-2.

Sarah Irwin, Slobodan P. Simonovic and Niru Nirupama (2016). Introduction to ResilSIM: A Decision Support Tool for Estimating Disaster Resilience to Hydro-Meteorological Events. Water Resources Research Report no. 094, Facility for Intelligent Decision Support, Department of Civil and Environmental Engineering, London, Ontario, Canada, 66 pages. ISBN: (print) 978-0-7714-3115-9; (online) 978-0-7714-3116-6.

Tommy Kokas, Slobodan P. Simonovic (2016). Flood Risk Management in Canadian Urban Environments: A Comprehensive Framework for Water Resources Modeling and Decision- Making. Water Resources Research Report no. 095. Facility for Intelligent Decision Support, Department of Civil and Environmental Engineering, London, Ontario, Canada, 66 pages. ISBN: (print) 978-0-7714-3117-3; (online) 978-0-7714-3118-0.

Jingjing Kong and Slobodan P. Simonovic (2016). Interdependent Infrastructure Network Resilience Model with Joint Restoration Strategy. Water Resources Research Report no. 096, Facility for Intelligent Decision Support, Department of Civil and Environmental Engineering, London, Ontario, Canada, 83 pages. ISBN: (print) 978-0-7714-3132-6; (online) 978-0-7714-3133-3.

Sohom Mandal, Patrick A. Breach and Slobodan P. Simonovic (2017). Tools for Downscaling Climate Variables: A Technical Manual. Water Resources Research Report no. 097, Facility for Intelligent Decision Support, Department of Civil and Environmental Engineering, London, Ontario, Canada, 95 pages. ISBN: (print) 978-0-7714-3135-7; (online) 978-0-7714-3136-4.

R Arunkumar and Slobodan P. Simonovic (2017). General Methodology for Developing a CFD Model for Studying Spillway Hydraulics using ANSYS Fluent. Water Resources Research Report no. 098, Facility for Intelligent Decision Support, Department of Civil and Environmental Engineering, London, Ontario, Canada, 39 pages. ISBN: (print) 978-0-7714-3148-7; (online) 978-0-7714-3149-4.

Andre Schardong, Slobodan P. Simonovic and Dan Sandink (2017). Computerized Tool for the Development of Intensity-Duration-Frequency Curves Under a Changing Climate: Technical Manual v.2.1.

Water Resources Research Report no. 099, Facility for Intelligent Decision Support, Department of Civil and Environmental Engineering, London, Ontario, Canada, 52 pages. ISBN: (print) 978-0-7714-3150-0; (online) 978-0-7714-3151-7. 58

Andre Schardong, Slobodan P. Simonovic and Dan Sandink (2017). Computerized Tool for the Development of Intensity-Duration-Frequency Curves Under a Changing Climate: User's Manual v.2.1. Water Resources Research Report no. 100, Facility for Intelligent Decision Support, Department of Civil and Environmental Engineering, London, Ontario, Canada, 52 pages. ISBN: (print) 978-0-7714-3152-4; (online) 978-0-7714-3153-1.

Ayushi Gaur, Abhishek Gaur and Slobodan P. Simonovic (2017). Modelling of High Resolution Flow from GCM Simulated Runoff using a Mesoscale Hydrodynamic Model: CAMA-FLOOD. Water Resources Research Report no. 101, Facility for Intelligent Decision Support, Department of Civil and Environmental Engineering, London, Ontario, Canada, 44 pages. ISBN: (print) 978-0-7714-3154-8; (online) 978-0-7714-3155-5.

Jingjing Kong and Slobodan P. Simonovic (2017). Multi-hazard resilience model of an interdependent infrastructure system. Water Resources Research Report no. 102, Facility for Intelligent Decision Support. Department of Civil and Environmental Engineering, London, Ontario, Canada, 99 pages. ISBN: (print) 978-0-7714-3158-6; (online) 978-0-7714-3159-3.

Andre Schardong, Slobodan P. Simonovic and Dan Sandink (2018). Computerized Tool for the Development of Intensity-Duration-Frequency Curves Under a Changing Climate: Technical Manual v.3. Water Resources Research Report no. 103, Facility for Intelligent Decision Support, Department of Civil and Environmental Engineering, London, Ontario, Canada, 67 pages. ISBN: 978-0-7714-3107-4.

Andre Schardong, Slobodan P. Simonovic and Dan Sandink (2018). Computerized Tool for the Development of Intensity-Duration-Frequency Curves Under a Changing Climate: User's Manual v.3. Water Resources Research Report no. 104, Facility for Intelligent Decision Support, Department of Civil and Environmental Engineering, London, Ontario, Canada, 80 pages. ISBN: 978-0-7714-3108-1.

Schardong, A., S. P. Simonovic and H. Tong (2018). Use of Quantitative Resilience in Managing Urban Infrastructure Response to Natural Hazards: A Web-Based Decision Support Tool - ResilSIMt. Water Resources Research Report no. 105, Facility for Intelligent Decision Support, Department of Civil and Environmental Engineering, London, Ontario, Canada, 112 pages. ISBN: 978-0-7714-3115-7.

Feitoza Silva D. and S. P. Simonovic (2020). Development of Non-Stationary Rainfall Intensity Duration Frequency Curves for Future Climate Conditions. Water Resources Research Report no. 106, Facility for Intelligent Decision Support, Department of Civil and Environmental Engineering, London, Ontario, Canada, 48 pages. ISBN:.

Braden, J. and S.P. Simonovic (2020). A Review of Flood Hazard Mapping Practices across Canada. Water Resources Research Report no. 107, Facility for Intelligent Decision Support, Department of Civil and Environmental Engineering, London, Ontario, Canada, 64 pages. ISBN:.

Patrick A. Breach and Slobodan P. Simonovic (2020). ANEMI 3: Tool for investigating impacts of global change. Water Resources Research Report no. 108, Facility for Intelligent Decision Support, Department of Civil and Environmental Engineering, London, Ontario, Canada, 134 pages. ISBN: